

# **SPATIAL STATISTICS AND SUPER RESOLUTION MAPPING FOR PRECISION AGRICULTURE USING VHR SATELLITE IMAGERY**

ARUN POU DYAL  
February, 2013

SUPERVISORS:  
Ir. Prof. Alfred Stein  
Dr. Valentyn Tolpekin



# **SPATIAL STATISTICS AND SUPER RESOLUTION MAPPING FOR PRECISION AGRICULTURE USING VHR SATELLITE IMAGERY**

**ARUN POUDYAL**

Enschede, The Netherlands, [February, 2013]

Thesis submitted to the Faculty of Geo-Information Science and Earth  
Observation of the University of Twente in partial fulfilment of the  
requirements for the degree of Master of Science in Geo-information Science  
and Earth Observation.

Specialization: Geoinformatics

## **SUPERVISORS:**

Prof.Dr.Ir. Alfred Stein (Supervisor)

Dr. Valentyn Tolpekin (Second Supervisor)

## **THESIS ASSESSMENT BOARD:**

Prof.Dr.Ir. M.G. Vosselman (Chair)

Dr.Ir. L. Kooistra (External Examiner, Wageningen UR)

#### DISCLAIMER

This document describes work undertaken as part of a programme of study at the Faculty of Geo-Information Science and Earth Observation of the University of Twente. All views and opinions expressed therein remain the sole responsibility of the author, and do not necessarily represent those of the Faculty.

## ABSTRACT

This research focuses mainly on exploring possibilities of SRM for identification of row crop structure for a potato field from VHR satellite image. For this purpose, anisotropic prior window of size 3 was implemented in a rotated SRM grid of size 20m X 20m for a non-integer scale factor value. Further it presents possible methods for exploiting spatial variability within farm using SRM classification results. Knowledge of spatial variation within farm can support farmers in decision making for better application of herbicide, manure and pesticides. This is more comprehensively addressed by management toolkit. Finally, this study explores possibilities for including SRM results into precision crop management for better decision making leading to fulfilment of specific goals of farmers.

The dataset used for this study is the WorldView 2 imagery of date 23 July 2012. The main aim of using VHR satellite image is to explore the possibility of available highest resolution sensors for row detection. Considering the effect of mixed pixels within the smaller study area, this study is challenging in terms of feature recognition. It was found that the SRM with high emphasis on spatial contextual information from prior model and spectral information from imagery is able to detect row structure prominently even for relatively complex scenes with high mixed pixels. Higher accuracy can be achieved for the detected rows with a balance of parameters for smoothness and spectral information.

Results show that smoothness parameter values  $\lambda$  0.9 and  $\lambda_{\text{pan}}$  0.5 provide optimal solutions with slower simulated annealing parameters  $T_o$  2 and  $T_{\text{upd}}$  0.99 produced continuous row structure. The main finding of this research is that the higher accuracy can be achieved in row detection with anisotropic prior window and with slower simulated annealing. The experimental results justified that lowest energy corresponds to highest accuracy and hence the developed model favours correct solution by giving high probability to classification with high accuracy at slower annealing. Further this study shows that field level variation can be observed by combining the SRM posterior energy with NDVI to help farmers for better decision in application of manure and pesticides.

## ACKNOWLEDGEMENTS

I express my sincere gratitude to my supervisor Prof. Dr. Alfred Stein for his continuous encouragement, invaluable comments and suggestions to me for completion of this work. I extend my sincere gratitude to my second supervisor Dr. V. A. Tolpekin for taking this work to the level higher than my expectations. I highly appreciate his careful comments, suggestions and support to me in each step during this work.

Further I would like to thank farmers of Het Bildt municipality specially farming company owner Mr. G.K. van der Werff for providing me useful information on the farming methods and lending me opportunity of field visit for observations and measurements. I also would like to thank Folkert de Vries, Alterra Wageningen UR for providing me useful information and Petra Budde, Technician, Web Coordinator, EOS department, ITC for her support during the image acquisition and processing.

I extend my sincere gratitude to me dear friend Sunil Thapa for his support during the field visit and throughout the work, my colleague and friend Miss Bayaramaa Enkhtur for providing me useful references in programming, Mr. Amare Degefaw for sharing relevant references, Mr. Chandra Prasad Ghimire for proof reading of my thesis and all my GFM colleagues and cluster mates for help and support in one way or other.

Finally, I thank my parents and family for continuous encouragement and support. I dedicate this work to my loving parents.

# TABLE OF CONTENTS

---

1.	Introduction	
1.1.	Motivation and problem statement .....	1
1.2.	Research Identification.....	2
1.2.1.	Research objective.....	2
1.2.2.	Research questions .....	3
2.	Literature review	
2.1.	Satellite remote sensing in precision agriculture .....	4
2.2.	Sub-pixel classification .....	5
2.2.1.	Super resolution mapping (SRM).....	6
2.2.2.	MRF based SRM .....	7
3.	Concept and methodology	
3.1.	Mixed pixel in VHR imagery (row crop scenario).....	9
3.2.	Class proportions and linear unmixing .....	9
3.3.	Class separability .....	10
3.4.	MRF model.....	11
3.5.	MRF based SRM.....	12
3.5.1.	Prior Energy Function.....	13
3.5.2.	Conditional Energy Function .....	14
3.6.	Energy optimization using simulated annealing .....	15
3.7.	Accuracy assessment.....	15
4.	Implementation	
4.1.	Project set up.....	17
4.1.1.	Study area .....	17
4.1.2.	Imagery selection.....	18
4.1.3.	Site identification and field visit .....	18
4.2.	Data preparation and pre-processing.....	19
4.3.	Evaluation of row crop structure and scale factor .....	21
4.4.	Class proportions estimation and class statistics .....	22
4.5.	Neighborhood window size .....	24
4.6.	SRM implementation with rotated grid .....	25
5.	Results	
5.1.	Analysis of row shift.....	26
5.2.	Experimental results on window size.....	27
5.3.	Experimental results on simulated annealing parameters.....	29
5.4.	Experimental results for optimal smoothness paramater.....	32
5.5.	Relating SRM results with crop management .....	33
6.	Discussion	
6.1.	Observation of the SRM results.....	37
6.2.	Using the SRM results for observing field variation .....	37
6.3.	Management approach for precision farming.....	39
6.4.	Answers to the research questions .....	41
7.	Conclusion and Recommendations	
7.1.	Conclusion .....	43
7.2.	Recommendations .....	43
	List of references .....	45

## LIST OF FIGURES

---

Figure 3.1: Neighborhood order and clique types.....	12
Figure 4.1: Study area showing Het Bildt municipality.....	17
Figure 4.2: Satellite image subsets and field observed photograph .....	19
Figure 4.3: Subset areas selected within the study area .....	19
Figure 4.4: 2D scatterplot for subset area 1 .....	20
Figure 4.5: 2D scatterplot for subset area 2 .....	20
Figure 4.6: Cross section and plan view of potato plantation structure. ....	21
Figure 4.7: Possible pixel arrangement of MS and PAN image pixels with SRM grid.....	22
Figure 4.8: Training pixels collected in MS and PAN image.....	22
Figure 4.9: Neighborhood window sizes for SRM implementation.....	24
Figure 4.12: Initial SRM (MLC of panchromatic image) and Reference image. ....	25
Figure 5.1: Row shift analysis plot at $\lambda$ 0.8 and $\lambda_{pan}$ 0.4 .....	26
Figure 5.2: Minimum energy trend at row shift of 0.16m.....	27
Figure 5.3: Optimized SRM for window size 1, Temperature update and Energy minimization curve. ....	27
Figure 5.4: Optimized SRM for window size 2, Temperature update and Energy minimization curve. ....	28
Figure 5.5: Optimized SRM for window size 3, Temperature update and Energy minimization curve. ....	28
Figure 5.6: Distribution of $k$ value at different values of $Tupd$ .....	30
Figure 5.7: Success rate for different values of $Tupd$ .....	31
Figure 5.8: Optimized SRM at $\lambda$ 0.9 and $\lambda_{pan}$ 0.5, Temperature update and Energy minimization curve	33
Figure 5.9: Variation of SRM posterior energy and Likelihood energies within the field .....	34
Figure 5.10: NDVI map overlaid on posterior energy of SRM .....	35
Figure 5.11: Ratio map, Soil classified from SRM symbolized with NDVI-energy ratio; Canopy classified from SRM symbolized with NDVI-energy ratio .....	36
Figure 6.1: Management toolkit for the management track of potatoes .....	40

## LIST OF TABLES

---

Table 4.1: List of available VHR optical sensors .....	18
Table 4.2: Spectral characteristics of WorldView2 image .....	18
Table 4.3: Training pixel statistics in multispectral and panchromatic image.....	23
Table 4.4: Class area proportions for soil and canopy.....	23
Table 5.1: Average values for 10 experiments of SRM implementation for different window size .....	29
Table 5.2: Summary of observations for <b>k</b> distribution at different values of <b>Tupd</b> .....	31
Table 5.3: Summary of results for different smoothness parameter values .....	32



# 1. INTRODUCTION

## 1.1. Motivation and problem statement

The importance of precision agriculture is increasing as it addresses three major trends in society for site specific optimization methods related to crop management, the environment and economic benefit. Precision agriculture considers the analysis of spatial and temporal variability of soil properties and crop productivity within systems like well-defined agricultural fields. Such an analysis is for example helpful in improving the efficiency of fertilizer application at specific locations in a farm field for better crop productivity and in this sense it is able to reduce environmental pollution due to excessive use of fertilizers (Hong et al., 2006). From the farmers' perspective, prior knowledge on variation that exists within the field can help to control the application of fertilizer based on location within farm (space) and crop growth stage (time). Considering a row crop scenario such as potato field, identifying rows of plants at and exploring spatial variability allows farmers to better understand the nature of the farm which leads to improved farm management practices in terms of application of manure and pesticides.

Satellite remote sensing imagery can assist a new generation of farmers to manage their croplands more effectively by determining the way their fields reflect and emit energy in the visible and infrared wavelengths (Wu et al., 2010). This helps in a dynamic management of croplands by monitoring a wide range of variables based on the crop and environmental status of the field. More specifically, multispectral high resolution remote sensing has a large influence on precision agriculture by its possibility to evaluate leaf area development and crop cover at the field scale (Clevers, 1997). In this way, identification and quantification of crop condition patterns and soil parameters are of the increasing importance to precision agriculture which may ultimately help in identifying management recommendations for farmers.

Classification of VHR multispectral imagery can provide a low cost solution for classification and identification of plants at the field level. A major problem with such imagery is the spatial-spectral trade-off between within class variability and spatial resolution. Furthermore, in heterogeneous areas, mixed pixels can occur in a single class leading to the modifiable area unit problem (MAUP). Considering these issues, hard classification methods may not be suitable for classification and identification of agricultural products at the plant level.

As a solution to aforementioned problem, this research considers super resolution mapping (SRM). SRM takes into account mixed pixels and thus provides more informative and appropriate representation (Tatem et al., 2003). SRM with linear spectral unmixing is often preferred where a mixed pixel is resolved into various class area proportions. Sub-pixel classification method though produces a composition of class fractions within individual pixels, but it cannot produce the actual spatial distribution of class fractions within a pixel to allow for a visual analysis and spatial variability of classification results (Kasetkasem et al., 2005). This issue of spatial distribution of class fractions within a pixel opens ideas for implementation of SRM.

SRM incorporates results obtained from sub-pixel classification to model the local spatial distribution of class fractions within each pixel for generation of fine resolution map using spatial optimization methods (Ardila et al., 2011). More specifically, SRM generates finer scaled hard classified maps as output considering the spatial distribution of class proportions within each pixel. Application of SRM in precision agriculture is expected to provide better identification of the plants and a better exploiting of local variation within homogeneous fields. Provided that it works, this may lead to a low cost and precise solution for timely information and improvement of on-going crop management practices in terms of application of manure and pesticides.

Context is important in the interpretation of visual information from imagery. It does not treat pixels separately but considers them to have a relationship with their neighbours. Therefore, such a relationship has spatial dependency (Kasetkasem et al., 2005). Markov Random Fields (MRFs) characterize contextual information by incorporating neighbourhood information and spatial structure in the form of homogeneous regions and assigns higher weight to those homogeneous regions than to isolated pixels. In this way it takes the spatial dependence into account during classification. MRF based SRM undertakes this idea of spatial dependence within the neighbourhood pixels throughout the generation of an SR map. This method is based on optimization algorithm where initially a sub pixel classification is done using coarse resolution image that is subsequently refined in an iterative refinement way.

## **1.2. Research Identification**

Current sensor technologies in agricultural sector are mainly focused on macro level agricultural monitoring (Wu et al., 2010). Hence, field scale crop and environmental parameters are restricted by limitations such as lack of high resolution, high accuracy and low cost technologies, this make it difficult to provide timely information in support of crop management and limiting the applications of precision farming. It also implies a strong research need for identification and implementation of low cost and high accuracy methods applied over the existing highest resolution imageries for better decision making in terms of existing precision agriculture practices.

Application of SRM in identifying row of plants at the field level from VHR imagery and exploring spatial variability in terms of crop health and soil can lead to identify specific management recommendations to the farmers for proper application of manure and pesticides. More specifically, the main focus of this research is on application of MRF based SRM at a VHR satellite image to identify rows of plants. The idea is that such a study can be used to explore spatial variability in terms of plant health and soil status located in polder regions of the Netherlands. It can be helpful to develop proper farm management recommendations in terms of application of manure and pesticides for protection of the environment, better crop management and economic benefit.

### **1.2.1. Research objective**

The main objective of this research is to implement MRF based SRM in a VHR satellite imagery of potato farm field in the Netherlands to identify the crop rows. Followings are the sub-objectives:

- Identification of a specific site with potato farm of crop growing season in the Het Bildt municipality in Friesland region of the Netherlands.
- Implementation of MRF based SRM in a VHR WorldView2 satellite image in specific site.
- Identification of rows of individual potato plants at field level using SRM.
- Interpretation of SRM results of identified rows to support better farm management practices in terms of application of manure and pesticides.

### 1.2.2. Research questions

- What are the basic criteria for site selection and identifying specific potato farms in the proposed site from satellite imagery?
- How to utilize prior knowledge of periodic spatial structure in SRM?
- What classes should be defined before implementation of SRM?
- What are the optimal parameter settings to obtain the best SRM result?
- Is it possible to identify individual rows of potatoes at field level using MRF based SRM?
- How to validate the classification output?
- What management recommendations can be identified for site specific management for better application of manure and pesticides?
- Does SRM provide more information on spectral variation of field than crop indicators such as NDVI?

## 2. LITERATURE REVIEW

This chapter covers the theoretical background and work that has been previously done specifically relevant to this thesis. The areas covered are issues and opportunities with VHR satellite imagery in precision farming, Sub-pixel mapping, MRF based SRM, geostatistical methods for variability analysis and precision crop management (PCM) at farmers level.

### 2.1. Satellite remote sensing in precision agriculture

Satellite remote sensing has been under investigation and use in crop monitoring and management from a long time. Relating the multispectral reflectance and temperature of crop canopy with the processes such as photosynthesis and evapotranspiration opened up the possibilities for implementing remote sensing in crop monitoring and management. Bauer (1985) identified conceptual framework for combining optical remote sensing data with soil, meteorological and crop data to model crop growth, yield and condition. Moreover, vegetation indices (VI) such as NDVI derived from canopy reflectance of multispectral imagery in wider wavebands can be combined with the climate variables to monitor growth response of plants (Hatfield et al., 1993). North-American Large Area Crop Inventory System (LACIE) and AgRISTARS programs showed successful results on use of RS data for crop identification, estimation of important crop canopy parameters and support in production forecasting. In this regard, Moran et al. (1997) reviewed existing methods and possibilities of image based remote sensing in precision crop management and suggested following opportunities with image based remote sensing:

- Multispectral images obtained in late crop growth season can be used to map crop yields and can be combined with crop growth models to predict final yield.
- Images obtained under conditions such as bare soil or full crop cover can be helpful in mapping spectral variability that may be useful in mapping management units.
- Multispectral images are helpful in identifying and monitoring various seasonally variable soil and crop conditions.
- Remote sensing observations can provide accurate input to determine causes of soil and crop variability across farmland thus supporting agricultural decision support system.

Further, a number of canopy state variables have been retrieved from satellite imagery by scientists. Most importantly, biophysical parameters such as fraction of absorbed photosynthetically active radiation (fAPAR) (Clevers, 1997), Leaf area index (LAI) (Bouman, 1995), fraction cover (fCOVER) (Bouman, 1995) and chlorophyll concentration (Haboudane et al., 2002) has been regarded as major canopy state variable incorporated in agro-ecosystem models. Other canopy variables such as mineral content, plant water content, Evapotranspiration, vegetation height and phenological information have also been successfully retrieved from satellite remote sensing for efficient monitoring and management of crops (Moran et al., 1997).

Leaf area index(LAI) is the total one sided green leaf area per unit ground area and is considered as important plant characteristics related to the photosynthesis that takes place in the green part of the plant (Clevers, 1988). LAI can be directly related to the crop biomass and can be an essential parameter in the analysis of spatial variability of crop conditions and productivity. Estimation of LAI from remote sensing observation requires accurate measure of soil reflectance which ultimately depends on soil moisture content. Considering the large effect of soil reflectance in LAI estimation for row crop fields such as potato, Clevers (1988) introduced an important assumption that the ratio between reflectance factors of bare soil in red and near infrared band are independent of the soil moisture content. This assumption was made based on the consideration that the reflectance decreases with increase in soil moisture content but the relative effect of the soil moisture content over the reflectance is similar at specific wavelength. On this basis, weighted difference vegetation index (WDVI) was derived which is the weighted difference between the corrected near infrared and red reflectance. WDVI was defined as a distance based vegetation index in which soil line was considered as a baseline for measure of distance and this distance was related to the measure of vegetation density. The estimation of LAI with this method outperformed method of LAI measured in field by traditional field sampling methods tested in an experimental farm of Agricultural Wageningen University. Further it emphasised WDVI as appropriate vegetation index instead of NDVI for LAI estimation in high crop density fields such as potato.

A more recent study by van Evert et al. (2012) on potato haulm killing adopting WDVI as an indicator of crop biomass showed that WDVI values obtained in a potato field using a ground based reflectance meter and with satellite based sensors are strongly and linearly related. This study showed the possibility to calculate herbicide rate considering the scale at which variable-rate application (VRA) is applied for potato haulm killing based on satellite image.

## **2.2. Sub-pixel classification**

VHR satellite imagery has been regarded as well suited for extraction of information on environmental features such as landcover at field scale. Despite the long history of research, potential of remote sensing for landcover classification is not fulfilled. In broader context, factors such as spectral bands, spatial resolution, atmospheric effects, methods used for image analysis and quality of reference data used for assessing classification accuracy limit the ability to accurately map information (Foody, 2002). Besides these factors, fundamental assumption made on remote sensing that ‘each pixel in image represents an area on earth surface with single class’ is unrealistic as the mixed pixels occur at each resolution level containing areas of more than one class(De Jong et al., 2006).

The proportion of mixed pixels in an image is the function of properties of sensor spatial resolution and landcover class composition on ground. Generally, this proportion increases with the decrease in spatial resolution (Campbell, 2002) but at finer resolution level in vegetated areas, the class constituent parts such as soil and canopy become more important for identification and as a result within class variability increases causing mixed pixel effect (De Jong et al., 2006). In heterogeneous area such as potato field, this effect is more since the mixed pixels occur in a single class causing modifiable area unit problem (MAUP). Thus without solving the problem of mixed pixels, the analysis of VHR satellite imagery for landcover classification can become highly unrealistic.

Hard classification methods consider each pixel in the image to consist one class assuming the pixels are pure which may not be appropriate considering the mixed pixel effects. The solution to this can be soft classification methods such as sub-pixel classification with linear spectral unmixing. Soft classification approach considers the scale and spatial variation issues and assigns labels to each pixel with the class area proportions thus addressing the mixed pixel effect (De Jong et al., 2006). A number of studies have been carried out on soft classification applied to remote sensing image. Most prominently, linear mixture model (Foody et al., 1994), neural networks (Atkinson et al., 1997) and support vector machines (Brown et al., 1999). All these methods prove to be more accurate than hard classification in terms of possibility for prediction of class proportions within each pixel, however lack the possibility of determining spatial location each landcover class within pixel (Richards et al., 2005). This requirement of spatial location of the class fractions within each pixel opens up the idea for super-resolution mapping (SRM).

### 2.2.1. Super resolution mapping (SRM)

Super resolution mapping (SRM) produces hard classification maps at resolution finer than the input imagery using spatial optimization methods (Atkinson, 2009). This method assumed the spatial dependence between the neighbourhoods pixels rely on the distance as the pixels closer together have similar values than the distant ones. However, the problem of determining the best possible location of class fractions within a pixel remains.

In literature, various methods have been proposed for SRM which mainly fall under two categories. The first is the regression type algorithms using geostatistical methods (Boucher et al., 2008), linear mixture model (Verhoeve et al., 2002) and feed-forward back propagation artificial neural network (ANN) (Mertens et al., 2004). Being the regression based approach, these methods are suggested to be fast as they do not involve iteration and they are able to determine uncertainty by estimating the prediction variance provided by the model. The second type are based on spatial optimization methods which mainly include algorithms such as spatial pixel swapping (Atkinson, 2005), simulated annealing (Atkinson, 2004), Hopfield neural network (Tatem et al., 2001).

Considering the above methods and implementation of it over VHR satellite imagery, very few studies have considered the potential contribution of panchromatic information for classification purpose (Ardila et al., 2011). These methods are more dependent on the class fractions generated from sub-pixel classification techniques such as linear spectral unmixing (Atkinson, 2009), thus limiting the scope of SRM to the quality of class fractions generated from sub-pixel mapping. Considering the application of the SRM over potato farm, sub-pixel mapping with linear unmixing cannot be preferred due to the existence of large spectral variance in the spectral response of the crop canopy crowns. This large variance makes the classes less separable. Instead, using MLC of panchromatic image as initial SRM proved that SRM map was not constrained by initial class-fraction map and hence produced better results (Ardila et al., 2011).

Considering the aforementioned issues, Markov random field (MRF) based SRM can be considered as appropriate alternative as this method can be useful to exploit multispectral and panchromatic information of VHR imagery and optimize the correlation between pixels of fine classified map. With recent modification and updates, this method is independent of results obtained from sub pixel mapping classification with linear spectral unmixing or other pansharpening methods (Ardila et al., 2011).

### 2.2.2. MRF based SRM

Kasetkasem et al. (2005) introduced alternative approach to map landcover based on MRF models at spatial resolution finer than the original image by taking into account contextual information. This method considers spatial dependence within and between pixels in the form of weight assigned to the pixels in a particular spatial structure (neighbourhood) based on probability. Raw coarse resolution images are used to generate sub-pixel classification which is iteratively refined to characterize the spatial dependence of neighbourhood pixels. The major assumptions of this method are:

- Mixed pixels can only occur in coarse resolution multispectral image.
- Super resolution map (SR map) has MRF property (Positivity, markovianity and homogeneity: described in methods chapter).
- Spectral values of classes in panchromatic image follow multivariate normal distribution.

The implementation was done by generating initial SRM from fraction images and then optimizing results by iterative pixel updating. For this process, neighbourhood window size was required to determine for labelling of central pixel. It considered the fixed neighbourhood window of the second order for any scale factor which limited the effectiveness of this method working at any scale factor (Kassaye, 2006). Another limitation of this method was dependency on the ground truth data for estimating the weight given to the neighbourhood pixels which may not be possible to obtain for every image.

Kassaye (2006) further studied MRF based SRM method introduced by Kasetkasem et al. (2005) for assessing the suitability of method for land cover mapping. The major modification was done for possibility of using variable neighbourhood size window in for different scale factors. Another modification was done on Gibbs parameter estimation where the weight assigned to each pixel were estimated using distance from the central pixel. This approach was tested in synthetic image and remote sensing data and the results showed higher accuracy value for synthetic data compared to real data. The justification to this was given as the possibility for exact estimation of mean and covariance matrices in the synthetic image and lack of proper reference data for remote sensing image thus propagating the quantitative error for the real image. Some other important findings from this study were:

- The optimal value of smoothing parameter varies with the type of scene and the class separability. Over smoothing effect or noisy appearance was observed if the smoothing parameter was not assigned properly.
- Quality of SRM decreases with increasing scale factor. The reason being increase in fraction of mixed pixels within coarse resolution pixel with the increase in scale factor.
- Class separability and number of classes have significant effects on quality of SRM thus choice of smoothing parameter value should be based on minimum class separability.

Tolpekin et al. (2009) studied effects of class separability on SRM accuracy using synthetic image and concluded that the SRM quality largely depends on smoothness parameter, scale factor and class separability. This study demonstrated that for each combination of scale factor and class separability, optimal value of smoothness parameters exist and thus higher classification accuracy can be achieved even for poorly separable classes with proper parameter combinations. This study recommended applicability of MRF based SRM to larger set of images with class separability ranging from poor to excellent.

Ardila et al. (2011) extended the previous work on MRF based SRM and implemented for tree crown identification in urban area in Enschede, Netherlands. This study used local optimization algorithm for labelling of tree crown pixels by defining objective energy function for conditional probabilities of panchromatic and multispectral images. This method exploited the information from multispectral and panchromatic images without relying on linear unmixing or other pansharpening methods. The obtained results outperformed results achieved from other methods such as maximum likelihood classification (MLC) and support vector machines (SVM). This method addresses issues on the insufficient spatial resolution in image classification by incorporating panchromatic information as well as within class variance in VHR imagery. Overall, this method represents the recent developments in MRF based SRM implemented over VHR satellite imagery and thus opens up the possibilities for implementing this approach at finer spatial scale such as in precision agriculture.

### 3. CONCEPT AND METHODOLOGY

This chapter describes the conceptual background of the methodology used to fulfil the specified objectives of the work. Section 3.1 describes the effect of mixed pixels in VHR imagery in row crop field. Theoretical background on class proportion estimation and class separability are presented in section 3.2 and 3.3. Theory on MRF models, MRF based SRM adopted for this research along with optimization process and accuracy assessment processes are described in section 3.4, 3.5, 3.6 and 3.7 respectively.

#### 3.1. Mixed pixel in VHR imagery (row crop scenario)

Geographical features in earth surface are heterogeneous and representation of these features in image is influenced by spatial scale and resolution of the remote sensing system. Spatial resolution of image is controlled by pixel size and determined by IFOV of the sensor system. Mixed pixel occur when the IFOV of the sensor falls in more than one class of geographic features in ground thus single pixel may represent more than one spectrally different landcover types. The radiance detected by the sensor is from the heterogeneous ground surface. As a result, the pixels generally contain more than one ground cover classes of mixed pixels.

Crops that are planted in rows have spectral reflectance primarily for two classes: crop canopy and soil. Considering the highest resolution VHR sensor such as WorldView 2 with spatial resolution (GSD) of 0.5 m capturing row crop imagery of potato plant with row spacing of 0.8 m, the possibility of occurrence of mixed pixel is high. Depending upon the row alignment in field and pixel orientation in the imagery, one pixel may contain more than one class with unknown class area proportions. Further, crop growth stage at the time of imagery capture also has effects on occurrence of mixed pixels. This effect depends on factors such as crop canopy gap between and within rows, degree of interlocking between individual plants, interlocking between rows and sun angle. Considering these issues, mixed pixels cannot be mapped by conventional methods. Hence, techniques such as soft classification approach with class proportion estimation are a critical step forward for successful classification.

#### 3.2. Class proportions and linear unmixing

Conventional hard classification methods adopt one-class-per-pixel techniques which are found to be inappropriate. The reason is the existence of mixed pixels at any spatial resolution. Soft classification techniques address the mixed pixel issue thus making it possible to classify the land cover features that are smaller than a pixel. However, the challenge here is to identify proportions of the pure components of classes that are present in the field of view of a sensor that causes mixed pixel effect (Kassaye, 2006). This proportion of class fractions are estimated by determining the pure spectral class components (endmembers) using techniques such as spectral mixture modelling. Linear mixture model (LMM) is commonly preferred for spectral mixture analysis. LMM is based on the assumption that received energy

at the sensor is the sum of energies received from each land cover class component. It assumes that there is no multiple scattering from land cover types. The amount of energy received from each class component is proportional to the ground area covered by each class. The mixture model is defined as:

$$Y = \sum_{i=1}^{N_{cl}} b_i v_i \quad (1)$$

Where  $b_i$  is vector of landcover proportions of class  $i$ ,  $v_i$  is matrix of number of bands ( $N_{bands}$ ) and number of classes ( $N_{classes}$ ) that denotes spectra of pure pixels in each landcover class. It is determined from pure training areas. After defining the spectra of pure pixels (endmember spectra), mixture model can be used to estimate the class compositions of a pixel with following constraint:

$$\sum_{i=1}^{N_{cl}} b_i = 1 \text{ and } 0 \leq b_i \leq 1 (i = 1, \dots, N_{classes}) \quad (2)$$

For error minimization, the number of spectrally pure endmembers must be less than number of image bands to allow unique solution.

### 3.3. Class separability

For a successful classification, spectral distance between two classes should be distinct in the feature space. This distinction should be such that the values within one cover type should be close together while values of different classes should be well separated. In this regard, Euclidean distance is the simplest class separability measure. It defined as the linear spectral distance between the mean vectors of each pair of signatures in the feature space.

Advanced measures of separability consider statistics of classes such as mean vectors and covariance of the training data. Divergence is the commonly used class separability measure based on the degree of overlap between the class statistics such as mean and covariance matrices. The value of divergence increases with increase in separation between classes. It has the quadratic nature which increases largely with increase in small separation between classes which may lead to false classification accuracy. Divergence is defined as follows with  $\alpha$  and  $\beta$  as classes,  $\mu$  as class mean and  $C$  as the covariance:

$$D_{\alpha\beta} = \frac{1}{2} (\mu_{\alpha} - \mu_{\beta})' (C_{\alpha}^{-1} + C_{\beta}^{-1}) (\mu_{\alpha} - \mu_{\beta}) + \frac{1}{2} Tr[(C_{\alpha} - C_{\beta})' (C_{\beta}^{-1} + C_{\alpha}^{-1})] \quad (3)$$

Transformed divergence ( $TD$ ) is the most commonly used class separability measure which has exponential nature and avoids large fluctuations with smaller change in class separation distance. It incorporates covariance with weight for determining the distance between class means thus higher value suggest well separable classes with greater statistical distance between the class means. Transformed divergence is defined with respect to divergence as:

$$TD_{\alpha\beta} = 2 \left[ 1 - \exp \frac{-D_{\alpha\beta}}{8} \right] \quad (4)$$

The value of  $TD$  ranges from 0 to 2 and the probability of correct classification increases with increase in value of  $TD$ .

### 3.4. MRF model

Bayesian classification approach shows combination of prior and conditional probability density functions in terms of maximum a posteriori (MAP) criteria. In maximum likelihood image classification, the class conditional probability density function (pdf) is modelled by Gaussian distribution. However, the prior pdf are generally overlooked which may cause loss of information. This can be improved by incorporating prior probability with class conditional probability to establish a maximum a posteriory (MAP) estimate. This is justified by Bayesian theorem as follows:

$$p(c|y, z) = \frac{p(c)p(y|z)}{p(y)} \quad (5)$$

Here,  $p(c)$  is the prior probability that the given pattern belongs to class  $c$ ,  $y$  is the set of observations and  $z$  is the given model,  $p(y|z)$  is the conditional probability of the set of observations for given model.

Context is defined as probability of existence of an object affected by their neighbours and is considered as major assumptions in modelling of prior probability (Tso et al., 2005). Context can be derived from three different dimensions: spectral, spatial and temporal. Interpretation of visual information is largely supported by contextual information as it allows elimination of possible ambiguities. With regard to context, pixels are not treated in isolation, rather considered to have spatial dependency between the neighbourhood pixels. Hence, modelling contextual classification can improve accuracy in classification as the relationship between pixel and its neighbourhood are treated as statistically dependent.

Markov random field (MRF) is a probabilistic model that provides an appropriate way to model contextual information. Let us consider  $X$  as a random field with random variables  $X_1, X_2, \dots, X_m$  defined on set  $Y$ , where  $x \in L$  ( $1 \leq i \leq m$ ) are the labels in  $X$ . MRF with respect to a neighbourhood system is defined as a random field, if its probability density function satisfies following criterions:

- Positivity:  $P(x) > 0$ , when this condition is satisfied, joint probability  $P(x)$  is uniquely determined by local conditional probabilities.
- Markovianity:  $P(x_i|x_{Y-i}) = P(x_i|x_{Ni})$ , this property states labelling of central pixel is dependent only on its neighbouring pixels.
- Homogeneity:  $P(x_i|x_{Ni})$  this property states that conditional probability for labelling a central pixel, given the neighbouring pixel is same regardless of relative location of the pixel.
- Isotropy: this property describes direction independence on labelling of central pixel. It states that for a central pixel, which is surrounded by neighbouring pixels of same order have same contributing effect in labelling.

Where,  $Y - i$  represents all pixels in set  $Y$  excluding pixel  $i$  and  $Ni$  denotes the neighbour of pixel  $i$ . The neighbourhood relation is arranged in the order of neighbours with following two important properties:

- A pixel can be its own neighbour.
- Labelling of pixel satisfy mutual neighbourhood relationship.

First order neighbourhood system has four pixels sharing a side with central pixel, as shown in figure 3.1(a). Second order neighbourhood system are the ones located in 4 corner boundaries with the pixel of interest figure 3.1(b) while higher order neighbourhood system expands on similar manner. A clique is a subset of a neighbourhood system, where all pairs of site are mutual neighbours. It can be single site, pair of sites or triple of neighbouring sites.

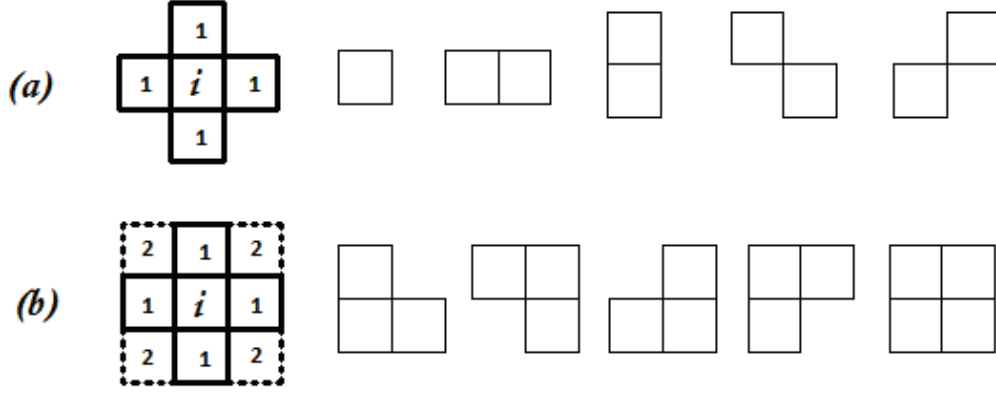


Figure 3.1: (a) The first-order neighbours of a pixel  $i$  with 4 pixels sharing side and different clique types associated with first order neighbourhood. Clique types are single site, horizontal and vertical neighbours and diagonal neighbours.

(b) The second-order neighbours of a pixel  $i$  with 4 corner pixels in boundary sharing side and different clique types associated with second order neighbourhood. Clique types are triplets and four neighbors. Source: (Tso et al., 2005)

As the order of neighbourhood system increases, the number of cliques also grows and hence computational complexity increases. Different clique types associated with first and second neighbourhood system are presented in figure 3.1(a) and 3.1(b). This contextual relationship between the neighbouring pixels is modelled with prior energy in MRF model.

### 3.5. MRF based SRM

MRF based SRM approach is considered appropriate for identifying potato plants for this study as it addresses major issues related to mixed pixels incorporating contextual information from prior model.

For classification of VHR imagery, SRM method considers multispectral image  $y$  with  $K$  spectral bands, spatial resolution  $R$  and pixel locations  $b_i \in B$ , where  $B$  is pixel matrix  $M_1 \times M_2$ . Further, it assumes panchromatic image  $z$  with finer spatial resolution  $r < R$  and defines Super-resolution map (SR map)  $c$  on the set of pixels  $A$  with resolution  $r$  that covers the same extent on ground as  $y$  and  $z$ . The scale factor of SR map is denoted by  $S$  as a ratio between coarse and fine resolution pixel size as  $S = \frac{R}{r}$ . Hence, each pixel  $b_i$  will contain  $S^2$  fine resolution pixels of  $a_{j|i}$  or  $a_j$  making the pixel matrix dimension as  $(SM) \times (SN)$ . This setup considers the number of pixels belonging to set  $A$  to be  $S^2$  times the number of pixels in set  $B$ .

Assuming the existence of multispectral imagery  $x$  with same spectral band as of  $y$  and spatial resolution  $r$ , which is not measured by satellite or equipment, image  $y$  and  $z$  can be considered as a spatial

and spectral degraded observations of image  $x$ . Further assumption is to consider every pixel in image  $x$  can be assigned to a unique class  $c(a_j) = \alpha$ , where  $\alpha = 1, 2, \dots, L$ . The relationship between images  $y$  and  $x$  can be established with the degradation model as,

$$y_k(b_i) = \frac{1}{s^2} \sum_{j=1}^{s^2} x_k(a_{j|i}) \quad (6)$$

$$z(a_{j|i}) = \frac{1}{K} \sum_k^K x_k(a_{j|i}) \quad (7)$$

The aim from above equations is not to estimate image  $x$  but to find SR map  $c$  that corresponds to MAP solution of  $p(c|y, z)$  for given observations in image  $y$  and  $z$ . This set up does not constraint the SR map  $c$  to an estimated class fraction from soft-classification but optimizes the SR map regarding spatial distribution of class labelled pixels and spectral properties of  $y$  and  $z$  images. Coming back to Bayes' theorem for computing posterior probability for images  $y$  and  $z$ ,

$$p(c|y, z) \propto p(c)p(y|c)p(z|c) \quad (8)$$

Assuming the images  $y$  and  $z$  to be conditionally independent, respective probabilities are represented by introducing energy functions such that it satisfy Gibbs distribution,

$$P(c) = \frac{1}{A_1} \exp\left(-\frac{U(c)}{T}\right) \quad (9)$$

$$P(y|c) = \frac{1}{A_2} \exp\left(-\frac{U(y|c)}{T}\right) \quad (10)$$

$$P(z|c) = \frac{1}{A_3} \exp\left(-\frac{U(z|c)}{T}\right) \quad (11)$$

$$P(c|y, z) = \frac{1}{A_4} \exp\left(-\frac{U(c|y, z)}{T}\right) \quad (12)$$

Here,  $T$  is constant called temperature,  $A_i$ ,  $i=1, \dots, 4$  are normalization constants which is independent of all possible configuration of  $c$ .  $U(c)$  is the prior energy function,  $U(y|c)$  and  $U(z|c)$  are the conditional energy functions while  $U(c|y, z)$  is the posterior energy function. Rewriting the Bayes formula in terms of energy function,

$$U(c|y, z) = \lambda U_c(c) + (1 - \lambda)(\lambda_p U(z|c) + (1 - \lambda_p)U(y|c)) \quad (13)$$

Here,  $\lambda$  is smoothness parameter for which the value ranges from 0 to 1 and it balances the contribution of prior and conditional energy to global energy.  $\lambda_p$  is an internal parameter for balancing contributions of two conditional energy functions for panchromatic and multispectral images. The above equation provides the MAP solution for the SR map  $c$  by minimizing energy with respect to  $c$ .

### 3.5.1. Prior Energy Function

Assuming SR map has MRF properties and considering equivalence between Gibbs random field and MRF, the MRF model for prior energy function can be expressed as the sum of pair site interactions,

$$U(c) = \sum_{ij} U(c(a_{j|i})) = \sum_{ij} \sum_{l \in N(a_{j|i})} w(a_l) I(c(a_{j|i}), c(a_l)) \quad (14)$$

Here,  $U(c)$  is the prior energy function of SR map,  $N(a_{j|i})$  is the neighbourhood system,  $U(c(a_{j|i}))$  is the local contribution of prior energy from pixel  $c(a_{j|i})$ ,  $w(a_l)$  is the contributing weight to prior energy from the neighbourhood pixel  $a_l \in N(a_{j|i})$  and  $I(\alpha, \beta)$  is equal to -1 if  $\alpha = \beta$  otherwise it is largest and is equal to 1. Contributing weight  $w(a_l)$  is modelled as:

$$w(a_l) = q \phi(a_l) \quad (15)$$

Here, parameter  $q$  ranges from 0 to  $\infty$  with higher values leading to smoother solution and  $\phi(a_l)$  is employed as an isotropic expression that depends only on the distance between pixels  $a_{j|i}$  and  $a_l$ . Based on assumption for representation of row as one pixel strip representing one row, positive weight of 1 is assigned to pixels along the row while negative weight 1 is assigned for pixels across the row.

This prior model gives preference to smooth SR map  $c$  and penalizes the pixels with different class label. Prior knowledge of periodic spatial structure of the farm field containing row plants such as average row distance, alignment and orientation of rows can be used in this regard. The conditional term incorporates distance between feature vector and mean vector with covariance matrix. The mean and covariance are modelled as linear mixture of mean and covariance matrices based on area proportions of land cover classes  $c(a_{j|i})$  inside pixel  $b_i$ .

### 3.5.2. Conditional Energy Function

For each landcover class, proximity of observed pixel values  $y$  and  $z$  are modelled by conditional energy function. Spectral value of  $x$  is assumed to be spatially uncorrelated and is modelled for class  $\alpha$  with Gaussian distribution. In this case, spectral values of  $y$  and  $z$  also follow the Gaussian distribution. The conditional term  $U(y|c)$  for multispectral image is defined as:

$$U(y|c) = \sum_i \frac{1}{2} [(M(y(b_i), \mu_i, C_i) + \frac{1}{2} \ln |\det C_i|)] \quad (16)$$

Here,  $(M(y(b_i), \mu_i, C_i))$  is the distance between feature vector  $y(b_i)$  and mean vector  $\mu_i$  with covariance matrix  $C_i$  known as Mahalanobis distance. Mean and covariance matrices are determined from training samples and refined from linear spectral unmixing based on area proportions for landcover classes  $c(a_{j|i})$  inside pixel  $b_i$ .

The conditional term for panchromatic image that follows normal distribution with mean  $v_\alpha$  and standard deviation  $\sigma_\alpha$  of class  $\alpha = c(a_{j|i})$  is,

$$U(z|c) = \sum_{ij} \frac{1}{2} \left[ \frac{(z(a_{j|i}) - v_\alpha)^2}{\sigma_\alpha^2} + \ln \sigma_\alpha^2 \right] \quad (17)$$

This model introduces spectrally degraded image  $z$  with equivalent resolution to image  $x$  and is adopted from Ardila et al. (2011). Here, multispectral and panchromatic energy models depend on spectral properties of crop canopy crown and soil background.

### 3.6. Energy optimization using simulated annealing

Criterion for pixel labelling based on Bayesian formulation is to find the MAP estimate which is a minimum energy solution in terms of MRF modelling. For an energy function such as strictly convex one with only one minimum point, basic search approach can be used to determine minimum energy. However, for non-convex energy function with more than one local minimum, true MAP estimate can only be obtained by finding a global minimum. Various iterative procedures exist such as simulated annealing (SA), iterative condition modes (ICM) and maximize of posterior marginal (MPM) for finding the global minimum by searching all local minimum. Considering the comparison study of these three methods for MAP estimate (Tso et al., 2005), simulated annealing proved to be better in terms of achieving lowest energy and highest classification accuracy. Hence, SA was chosen as appropriate method for energy optimization in this study.

Simulated annealing (SA) is a stochastic relaxation algorithm of iterative optimization based on the idea of liquid freeze or metal recrystallization. SA considers randomness (temperature) to decrease in iterative way to reach the minimum energy solution. The iterative energy optimization starts at initial high temperature at disordered stage and slowly cools down to an ordered stage based on a carefully defined criterion called cooling schedule. The process continues until the frozen state is reached where the temperature approaches to zero ( $T \rightarrow 0$ ). The optimization process runs with the predefined cooling schedule of  $T = T_o \times T_{upd}$  while, SA parameters initial temperature ( $T_o$ ) and updating schedule ( $T_{upd}$ ) control the process. High temperature refers to the state when large number of pixels has different values showing high randomness which increases probability of a pixel label being replaced by new class label. As the optimization continues, the algorithm tries to find the global minimum and a very small increase in energy is allowed. Finally the energy reaches at freezing point where no more pixels are updated representing the minimum energy solution. The algorithm updates pixel in a row wise scheme with three time updates for each temperature update value. The process stops if there is no pixel updates in these three consecutive iterations.

Any starting point of initial temperature ( $T_o$ ) is allowed. Random starting point may take additional iterations for convergence. SA iteratively minimizes energy function to Gibbs distribution with temperature decreasing to zero. According to Gibbs distribution as presented in equations 9 to 12, minimizing energy is equivalent to maximizing the probability of pixels being labelled with correct class. This leads to higher classification accuracy.

### 3.7. Accuracy assessment

Accuracy assessment in classification corresponds to the level of agreement between the class labels achieved from the classification model with the reference data. Comparison of results is done on class by class basis with the reference data. This helps to derive error matrix from which accuracy measures such as user accuracy, producer accuracy and overall accuracy can be derived. User accuracy is a measure of commission error which is obtained by dividing number of correctly classified pixels for each class with total number of pixels classified as that particular class. It determines the probability of classified pixels represents same class information on ground. Producer accuracy is a measure of omission error and is

obtained by dividing number of correctly classified pixels in each class by the total number of pixels in that class. The most common measure of accuracy is overall accuracy that represents the proportion of correctly classified pixels. It is obtained by dividing total number of correctly classified pixels by the number of pixels checked.

The above accuracy measures are derived based on principle diagonal of the error matrix which does not take into account off-diagonal elements.  $k$  coefficient is the measure of overall agreement between the classification and reference data that is derived from whole error matrix considering off-diagonal elements. For this study,  $k$  coefficient is used as accuracy measure for testing the performance of the model with optimal parameter values obtained from experimental analysis. Experiments are conducted to determine optimal settings of  $\lambda$  and  $\lambda_p$  values that identify row structure by determining their correspondence with the highest value of  $k$  coefficient.

## 4. IMPLEMENTATION

This chapter presents implementation approach adopted to fulfil the specified aims and objectives. Section 4.1 describes the initial setup that includes decisions made on choice of imagery, study area and site for implementation of SRM. Section 4.2 describes the pre-processing of imagery data and observations of descriptive statistics for the selected imagery subset. In further sections this chapter presents the decisions made on scale factor and target resolution of SRM, determination of class statistics and SRM implementation procedure.

### 4.1. Project set up

With the aim of identification of row crops from VHR satellite imagery, initial desk study was done to determine the possible study area within the Netherlands. Choice of VHR imagery of highest resolution available sensor and crop types to identify was also finalized in this study. Following subsections describe the detail procedures adopted for the initial setup of project:

#### 4.1.1. Study area

Agricultural farms in northern areas of the Netherlands are mostly known for production and marketing of crops such as potato, sugar beet, onion, oats and other cereal crops. Polder regions of low lying areas enclosed by dikes (embankments) are considered favourable for growth of potatoes. Potato crops are planted in rows and represent one of the largest volume of production and marketed crop of the Netherlands. Considering the large production volume and high possibility of identifying a potato farm in field, potato was chosen as the appropriate row crop for this study.

Het bildt is the municipality situated in the Friesland province in the north polder region of the Netherlands. This area is chosen as the study area as the northern region of the municipality predominantly contains row crops such as potato and sugar beet.



Figure 4.1: Study area showing Het Bildt municipality in the northern polder region of the Netherlands.

#### 4.1.2. Imagery selection

A review of available VHR optical sensors and satellite imaging libraries were conducted to identify proper sensor for the specific task. Following table shows list of currently available VHR optical sensors:

Sensor	GSD pan(m)	GSD MS(m)	Swathe nadir(km)	Channels
IKONOS2	0.82	4	11.3	Pan, MS
QuickBird	0.61	2.88	16.5	Pan, MS
OrbView3	1	4	8	Pan, MS
EROS B	0.7	-	7	Pan
KOMPSAT-2	1	1	15	Pan, MS
WorldView1	0.45	-	17.6	Pan
WorldView2	0.46	2.4	16.4	Pan, MS
GeoEye1	0.41	2.4	15.2	Pan, MS
Cartosat2	0.82	-	9.6	Pan

Table 4.1: List of available VHR optical sensors

WorldView2, GeoEye1 and Quickbird sensors were initially shortlisted based on the ground sampling distance (GSD) for panchromatic and multispectral imagery. For the choice of appropriate sensor and imagery, following criterions were followed:

- Latest imagery capture date with late growing season of potato plants (June to August) that increases possibility of fields containing full crop cover.
- At least 4 available bands with availability of NIR band.
- Completely free from cloud cover with nadir viewing angle.
- Full coverage of study area
- Considerations on image attributes such as sensor angle, azimuth and geometric parameters.

Based on these considerations, WorldView 2 image with 4 channels of multispectral data of 2m resolution and 1 channel of panchromatic data of 0.5m resolution was chosen as appropriate imagery for this study. The image acquisition date of the imagery is 23 July 2012 which matches to the possible maximum crop cover time. Following table shows spectral characteristics of WorldView 2 image:

Band	Description	Wavelength( $\mu$ m)	Resolution
Band 1	Blue	0.45 - 0.51	2
Band 2	Green	0.51 - 0.58	2
Band 3	Red	0.63 - 0.69	2
Band 4	NIR	0.77 - 0.89	2
Pan	-	0.45 - 0.80	0.5

Table 4.2: Spectral characteristics of WorldView2 image

#### 4.1.3. Site identification and field visit

Possible potato farm fields were initially identified and shortlisted in satellite imagery by visual interpretation. Confirmation of the selected site containing crop cover was made by Email and telephone queries with the agro-industries and farming agencies working in the field in production and marketing of crops. One day field visit was conducted on 06 October 2012 to 5 different shortlisted farm fields within the coverage area of satellite imagery. Following three major tasks were performed during the field visit:

- Initially identified sites in satellite imagery were verified in field for crop type.
- Potato crop field were identified and basic measurements were taken on inter-row spacing and plant spacing.

- Agricultural industries and farming agencies working in potato crop were visited and oral interview was conducted with the farmers.

Followings are some major observations from the field visit:

- Crops such as potatoes and sugarbeet are planted in rows and estimates of hundred thousand seeds per hectare are planted.
- Row distance 75 to 80 cm – for potatoes
- Plant distance 20 to 30 cm – for both potato and sugarbeet
- Potatoes are grown in different varieties based on the genetics. These varieties are produced by altering the seed type, amount of nitrogen and fertilizer application. A same field can contain different varieties of potatoes.
- In early growing season (May-June), the plant rows and soil can be seen clearly. In mid to high growing season (July-Aug), the interlocking of canopy increases and soil may not be clearly seen.
- The rotation of crop plantation is once in every three years.

From the above observations, subset imagery of potato farm field with full crop cover containing single variety of potato was chosen as the appropriate image for this study. Following figures show the selected subset imagery and field observed photograph of the site:

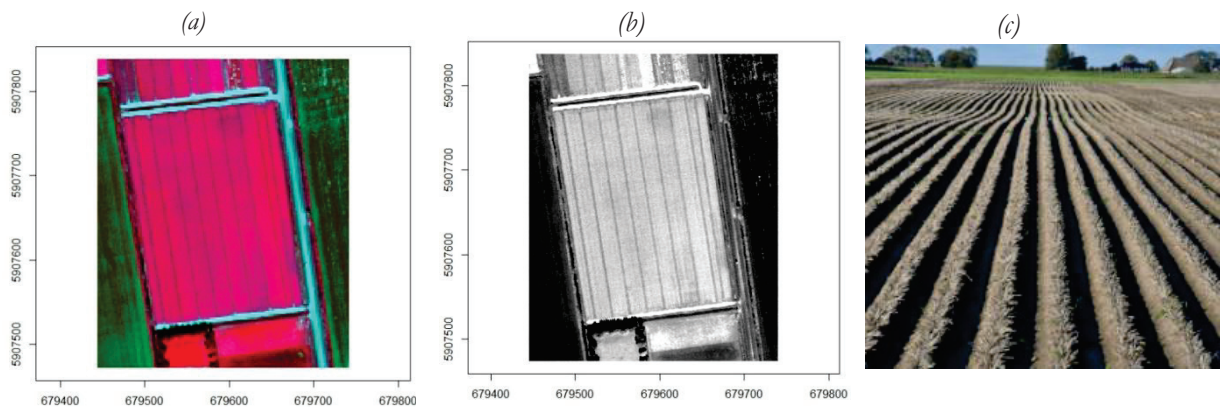


Figure 4.2: (a) Multispectral image subset of study area; (b) Panchromatic image subset of the study area; (c) Field observed photograph of potato showing plants ready for harvesting

## 4.2. Data preparation and pre-processing

As of the objective of this study is to identify plant rows, co-registration between the multispectral and panchromatic bands of chosen subset area is important. Considering the resampling involved in the process of co-registration and possible loss of spatial integrity of the data which may have adverse effects in SRM implementation, checking the requirement of co-registration between the panchromatic and multispectral data was the first step. This was done by pixel swipe tool in ENVI software. Further, locations of Ground control points (GCP) were collected manually in

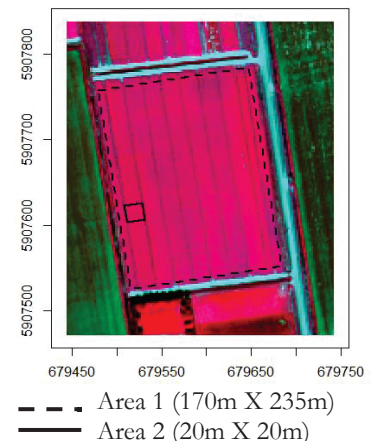


Figure 4.3: Subset areas selected within the study area

distinct locations of the multispectral and panchromatic subset image. These locations were verified based on the cursor value for x and y coordinates. The correlation between these 10 set of points were observed to be in the error limit of 0.014m which was considered well enough for SRM implementation. Considering this observation, image co-registration process was not considered necessary. WorldView2 imagery was provided in GeoTIFF file format with spatial reference of UTM zone 31 north spheroids and WGS 1984 datum. The panchromatic and multispectral bands necessary for SRM implementation are in same spatial reference and coordinate system. Thus, geometric correction and referencing of the imagery were not considered necessary.

Descriptive statistics of the multispectral and panchromatic bands were explored for two levels of subset areas within the selected image. Subset area 1 is a rectangular area of size 170m X 235m approximately covering the entire field. To ensure the area lies completely within the field, outer edges of the field are excluded by taking sufficient offset from the boundary. Subset area 2 is a rectangular area of size 20m X 20m that lies within the row strips. Following figures show the subset areas and scatterplot for the multispectral band of the subset areas:

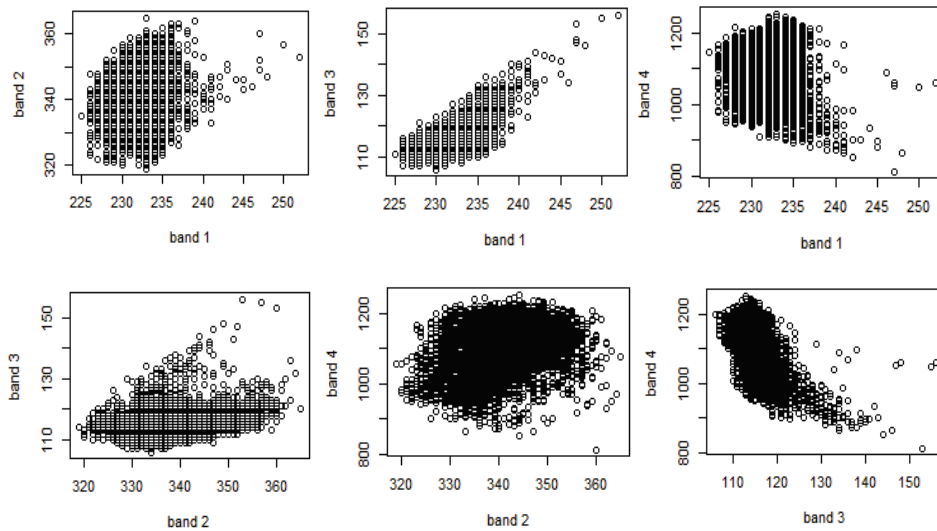


Figure 4.4: 2D scatterplot for subset area 1 showing distribution of DN values in different band combinations

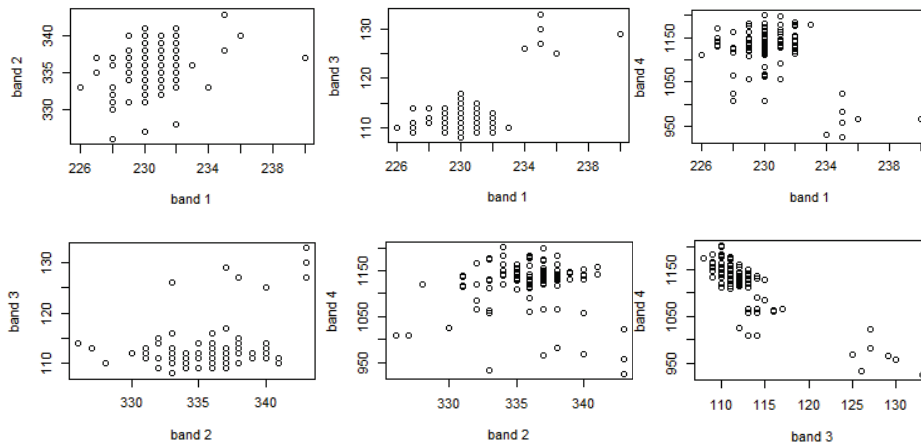


Figure 4.5: 2D scatterplot for subset area 2 showing distribution of DN values in different band combinations

The above 2D scatterplot for the subset area 1 and 2 show high possibility of mixed pixels which can be observed from the clustering amount between the DN values in different band combinations. Scatterplot of NIR (band4) and Red (band3) show a large clustering with a long tail suggesting high mixed pixels.

### 4.3. Evaluation of row crop structure and scale factor

Potato crop being one of the most produced crops in the Netherlands, are planted in ridges of soil rows prepared beforehand. From the field visit and interview of local farmers working in Het bildt, it was observed that spacing between rows depend on existing practice of local area, implementation process and variety of potato. Plantation spacing depends on the variety of potato, growing conditions and soil fertility. For this study, farm field containing one variety of potato with row spacing of 0.8m and plant spacing of 0.3m has been chosen and verified in field. Following figures show the structure of plantation and dimensions:

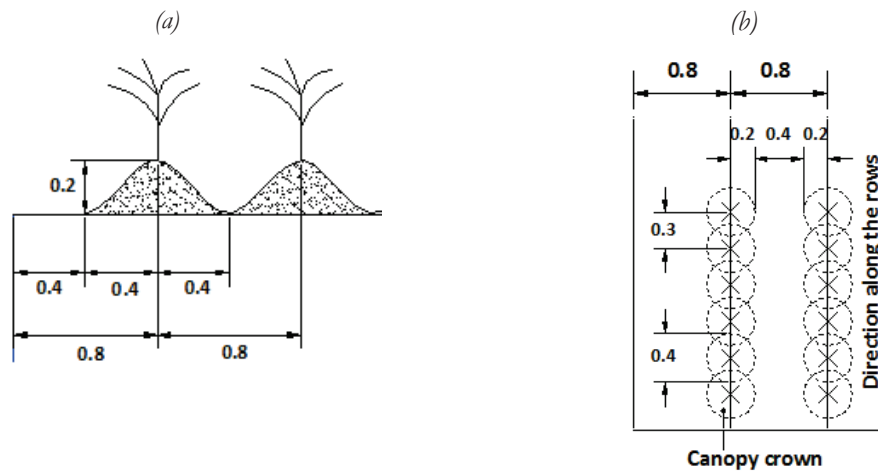


Figure 4.6: (a) Cross section view of potato plantation in row structure showing the spacing between rows; (b) Plan view of potato plantation in row structure shows plant crown size and distance between consecutive rows.

The dimensions showed in figure are observed in field and regarded as important considerations as a preliminary knowledge (prior knowledge) of the plantation structure. This knowledge is considered as important addition while interpreting image information. Visual interpretation of multispectral and panchromatic imagery show very little sign of possible rows. In such case, identification of rows considering the spectral information alone is unrealistic. Incorporation of prior information provides knowledge on row orientation, alignment and spacing and this knowledge were used to first identify the row structure in smaller subset imagery.

The output resolution of classification (target resolution) was decided based on analysing the pixel arrangement in multispectral and panchromatic imagery with the row structure. Following figure shows the arrangement of rows with respect to imagery pixels:

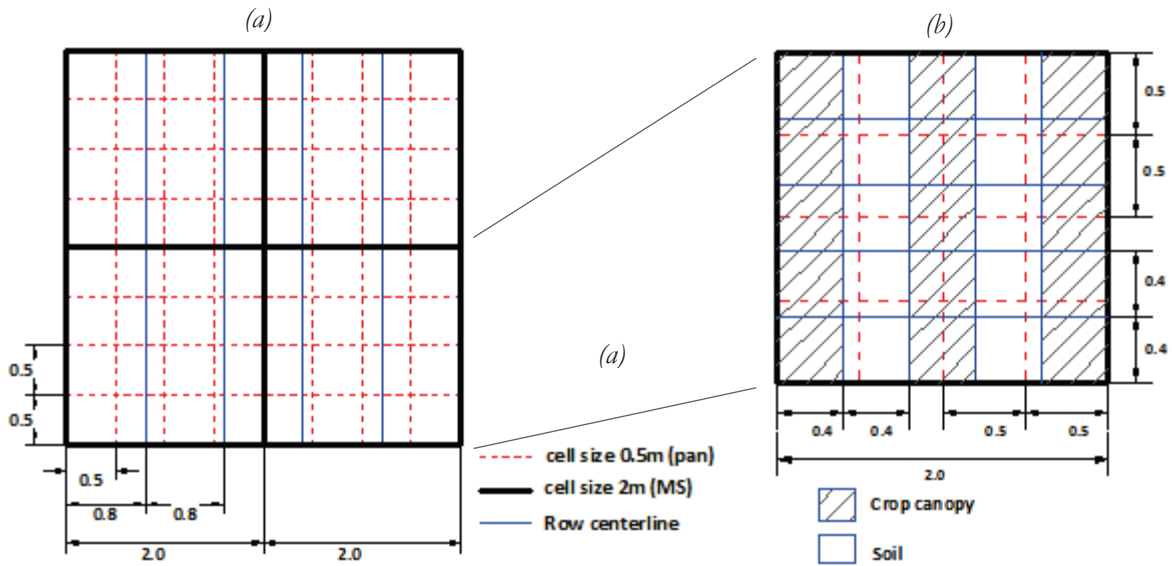


Figure 4.7: (a) Arrangement of multispectral and panchromatic image pixels with the row structure of spacing 0.8m; (b) Possible arrangement of row representation for SRM target resolution grid of 0.4m overlaid on cell size of 0.5m (pan) and 2m (MS).

Figure 4.7 shows possible arrangement of row centreline (blue) overlaid in multispectral cell size of 2m (black) and panchromatic cell size of 0.5m (red). Considering two major classes as crop canopy and soil, output resolution of 0.4 m was decided for correct representation of rows (figure on right). Here, each 0.4m track of cell along the row direction is supposed to represent crop canopy and soil classes in alternative order moving from left to right. For, this arrangement of representation of rows, following considerations were made:

- All fine resolution pixels of panchromatic image as well as output resolution are completely inside multispectral pixel of 2m.
- Target resolution pixels lying in the boundary with panchromatic image pixels consider nearest neighbour pixel from panchromatic image to acquire spectral information.

Based on above analysis for SRM target resolution of 0.4m and scale factor of 5 was considered appropriate for SRM implementation. However, during implementation, SRM coordinate grid was rotated with respect to the image grids by 9 degrees and hence, the scale factor value of 5 was revised to a non-integer number close to 5.

#### 4.4. Class proportions estimation and class statistics

For this study, two major classes are considered as crop canopy and soil. Considering high possibility of mixed pixels in the imagery, two set of training pixels were collected in panchromatic and multispectral image. Following figures show the collected of training pixels in multispectral and panchromatic image using ENVI software.

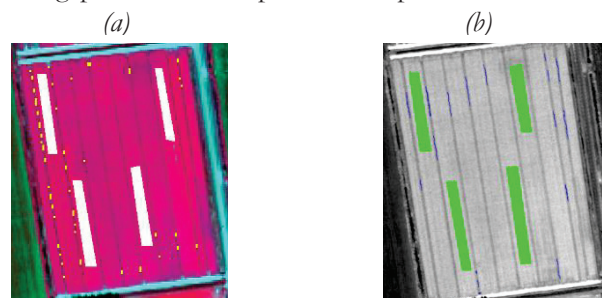


Figure 4.8: (a) Training pixels collected in multispectral image; (b) Training pixels collected in panchromatic image

Following table shows the number of training pixels collected in panchromatic and multispectral bands and their respective colours:

Training Class	Panchromatic		Multispectral	
	Color	No of Pixels	Color	No of Pixels
Mixed soil in canopy	Green	15379	White	879
Mixed soil in between strips	Blue	780	Yellow	77

Table 4.3: Training pixel statistics in multispectral and panchromatic image

From the above training classes, class statistics for mean and covariance matrices for multispectral image as well as mean and standard deviation for panchromatic image were determined. Further correction for soil in the training pixels is important as the collected training pixels still contain mixed pixels. Considering the imagery capture date of peak growing season of crop, factors such as degree of interlocking of plants as well as insufficient resolution of imagery can cause high possibility of identified training pixels being highly mixed. In such case, both the training classes of canopy and soil cannot be considered pure. To overcome this issue and to determine pure soil and canopy class statistics, linear mixture model was applied. Based on field verification and prior knowledge, following considerations were made for class proportions for soil and canopy before application of linear mixture model:

Training classes	Class proportions	
	Soil	Canopy
Mixed soil in canopy	0.5	0.5
Mixed soil in between strips	0.75	0.25

Table 4.4: Class area proportions for soil and canopy

Based on the above class proportions, following linear mixture model was applied to determine the pure class statistics for soil and canopy classes.

$$\mu_1 = \theta_1 \mu_s + (1 - \theta_1) \mu_c \quad (18)$$

$$\mu_2 = \theta_2 \mu_s + (1 - \theta_2) \mu_c \quad (19)$$

Here,  $\mu_1$  = Mean of mixed soil in canopy

$\mu_2$  = Mean of mixed soil in between strips

$\mu_c$  = Mean of pure canopy

$\mu_s$  = Mean of pure soil

$\theta_1$  = Class proportion for mixed soil in canopy

$\theta_2$  = Class proportion for mixed soil in between strips

Solving the above linear mixture model, pure class statistics for soil and canopy were derived. The corrected class statistics obtained from above are used in SRM implementation.

#### 4.5. Neighborhood window size

For this study, 3 different neighbourhood system windows are tested for probability of correct labelling of pixels to create prominent row structure that correspond to minimum energy solution. Number of maximum neighbours included for each neighbourhood system is given by:

$$N_{max} = (2 \times W_{size} + 1) \times 3 \quad (20)$$

Here,  $N_{max}$  is the number of maximum pixels included in neighbourhood window,  $W_{size}$  is the window size. For this neighbourhood system, following 3 window sizes is tested for minimum energy solution:

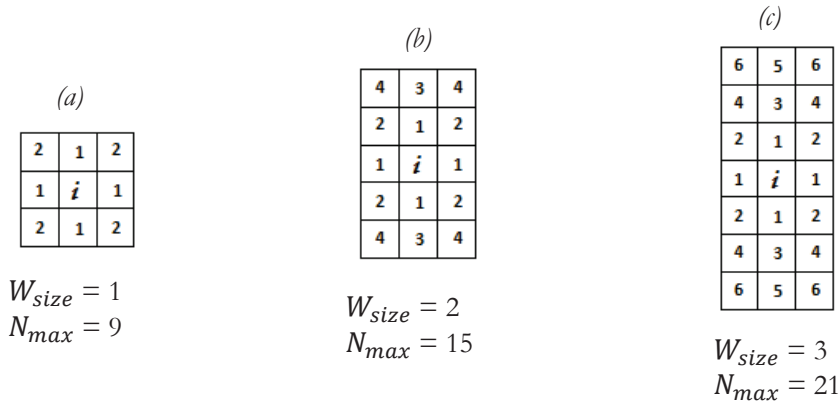


Figure 4.9: (a) Neighbourhood window of second-order for SRM implementation with window size 1 (b) Neighbourhood window of fourth-order for SRM implementation with window size 2 (c) Neighbourhood window of sixth-order for SRM implementation with window size 3

Isotropic property of MRF justifies property of direction independence where, surrounding neighbourhood pixels have same contributing effect on labelling the centre pixel (Iso et al., 2005). As the surrounding pixel have same contributing effect, this setup may not be suitable for the row representation. For target resolution 0.4m, this type of labelling may cause more homogeneous clusters without prominent row structure. In contrast, mutual neighbours along a pixel strip were assigned with positive weight 1 while the neighbours across the pixel strip with negative weight 1. Hence, anisotropic property of MRF was considered for assigning weight of pixels in neighbourhood with weight criterion as described in section 3.5.1.

#### 4.6. SRM implementation with rotated grid

As the multispectral and panchromatic imagery only show some hints of possible rows, rotation of imagery subset was avoided to reduce the problem of pixel resampling. SRM grid data frame was itself rotated to with respect to the grid of images. The rotation angle of 9 degrees was determined in imagery by measurement of row alignment direction with the vertical in ArcGIS software. The links between the pixels of rotated SRM grid and image pixels were established based on the geographic coordinates. For this, square foot print of multispectral image was taken as starting point such that centres of SRM pixels fall inside the square footprint. Considering scale factor approximately equal to 5, average  $S^2$  number of SRM pixels equals to 25 pixels in 1 multispectral image. The relation between multispectral pixel and SRM pixel was established based on geo-location. Relation between panchromatic image pixel of resolution 0.5m and SRM pixel of 0.4m was established based on one to one pixel assumption which considers the nearest centre of panchromatic image with SRM pixels. Considering the rotated grid of the SRM and non-rotated pixels of the image, this implementation was done for a non-integer scale factor value close to 5. SRM was implemented in the subset area of 50 X 50 pixels of size 20m X 20m for which MLC of panchromatic image was taken as initial SRM (Figure 4.12 a). Considering the small size of implementation area, spatial point data frame was chosen for better representation of pixels where one point represents one pixel of size 0.4m X 0.4m on ground. Reference image (Figure 4.12 b) was created based on the prior knowledge on row structure and position of alternate class of rows. To reduce the effect at boundary, two consecutive rows at the left and right side of the boundary were removed. To determine the best possible starting position of the rows within grid, row shift analysis was conducted along the direction orthogonal to plant rows. Shift value of 0.16m was determined for best possible position of rows within grid. Initial SRM was generated and iteratively optimization of energy was done using simulated annealing.

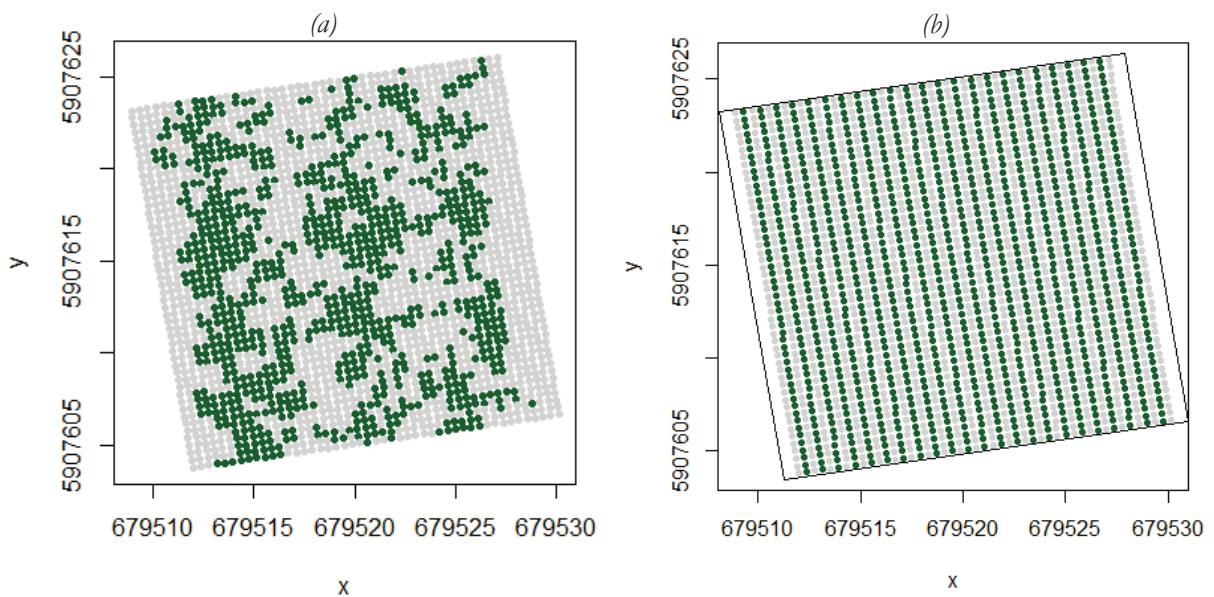


Figure 4.10: (a) Initial SRM (MLC of panchromatic image) (b) Reference image

## 5. RESULTS

This chapter presents the conducted experiments and results obtained from the implemented SRM model. Section 5.1 presents the experiments conducted and results obtained to determine the exact position of start of rows within the specified subset area of 20m X 20m. Section 5.2 shows the experiments conducted and results obtained for different neighbourhood window sizes and decisions made based on the observations. Section 5.3 presents experiments conducted on simulated annealing parameters for determining minimum energy solution. This section also describes observations of  $k$  statistics for different SA parameters along with process for evaluating performance of the model. Section 5.4 presents experiments conducted to determine optimal smoothness parameters for multispectral and panchromatic image and describe observations made from the experiment. Finally, section 5.5 shows possibilities of using SRM results for observing field variation.

### 5.1. Analysis of row shift

Determining location for appropriate position for crop rows within SRM grid is important for achieving correct labelling of pixels. According to Gibbs random distribution, probability of pixels being labelled with correct class is high when the posterior energy converges to a minimum solution which leads to higher classification accuracy. As MRF model follows Gibbs distribution, the idea of achieving minimum energy solution was adopted to determine the best possible position of rows for SRM grid. Entire SRM grid was shifted to one pixel corresponding to 0.4m with an incremental shift value of 0.04m in the direction orthogonal to the plant rows. This shift analysis was conducted for 5 different values of  $\lambda$  and  $\lambda_{pan}$  (0, 0.2, 0.4, 0.6 and 0.8) and energy trend was observed. Following figure shows the energy values at shift increment of 0.04m at  $\lambda$  0.8 and  $\lambda_{pan}$  0.4.

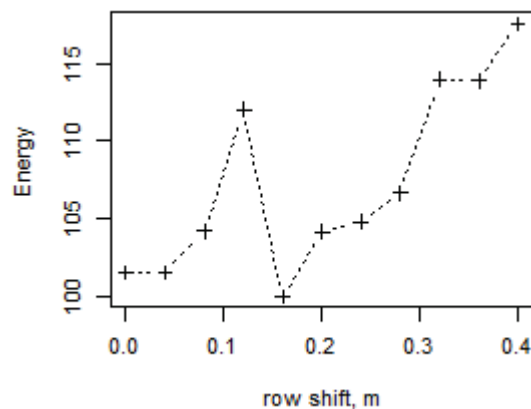


Figure 5.1: Row shift analysis plot at  $\lambda$  0.8 and  $\lambda_{pan}$  0.4 showing minimum energy at shift value 0.16m

Observation of above figure shows energy values are lowest at shift 0.16m. This trend was observed for all 5 combinations of  $\lambda$  and  $\lambda_{pan}$  thus all the combinations of parameter showed minimum energy at same shift of 0.16m. Based on this observation, row shift value of 0.16m was adopted as ideal shift that corresponds to the minimum energy solution. To determine the trend of minimum energy at different smoothness parameter settings, minimum energy trend was plotted at shift value of 0.16m.

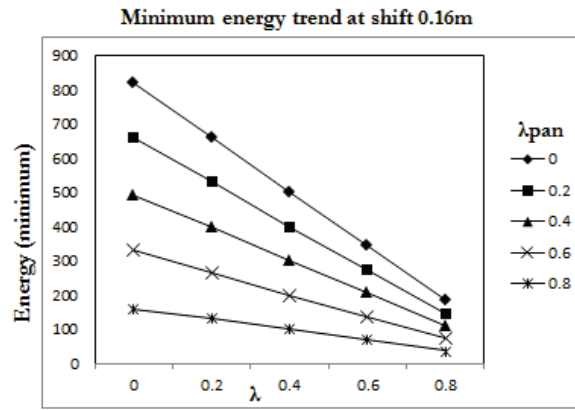


Figure 5.2: Minimum energy trend at row shift of 0.16m

The energy trend plot (Figure 5.2) shows the decreasing trend of minimum energy values with increase in values of  $\lambda$  and  $\lambda_{pan}$ . Energy decrease trend is linear for all parameter combinations which indicates that correct class labelling and better classification accuracy can be achieved at higher values of  $\lambda$  and  $\lambda_{pan}$ . This finding was also considered helpful for choosing the optimal smoothness parameter settings for multispectral and panchromatic image subset.

## 5.2. Experimental results on window size

Three neighbourhood windows of size 1, 2 and 3 were tested for quality detection of rows in terms of finding the minimum energy solution and  $k$  statistics. Experiments on window size were conducted for fixed values of smoothness parameters and simulated annealing parameters  $T_0$ . To explore the consistency of the row detection and to evaluate the reproducibility, each experiment was repeated for 10 times for same parameter settings. For this experiment, parameter values  $\lambda$  0.9,  $\lambda_{pan}$  0.5,  $T_0$  2 and  $T_{upd}$  0.9 were considered. Following figures show the optimized SRM, temperature minimization and energy optimization process for different window size.

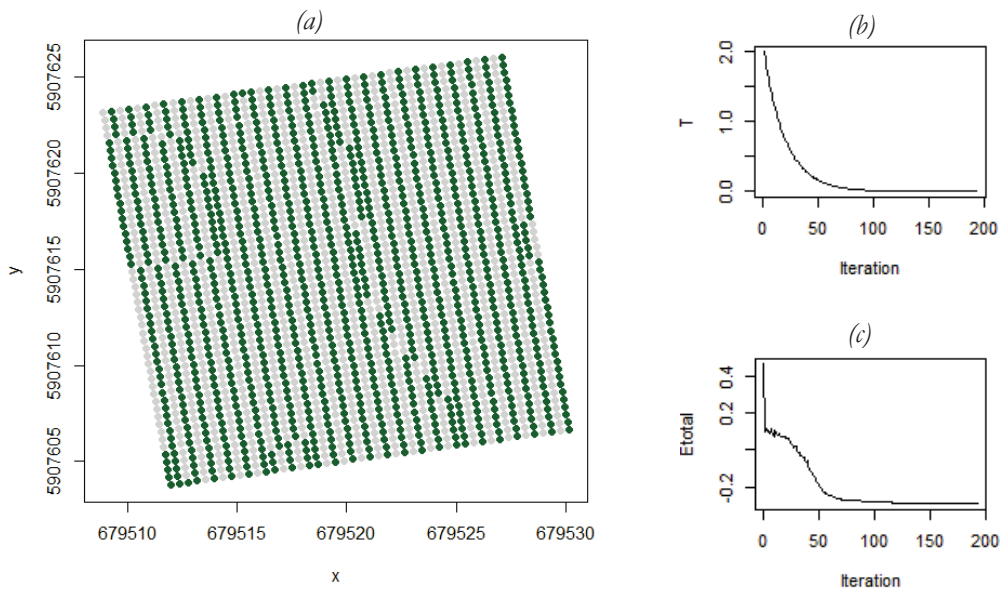


Figure 5.3: (a) Optimized SRM for window size 1 showing more break lines and overlaps between consecutive rows; (b) Temperature update (c) Energy minimization curve showing local minimum values as jumps and finally converging to global minimum value below -0.2.

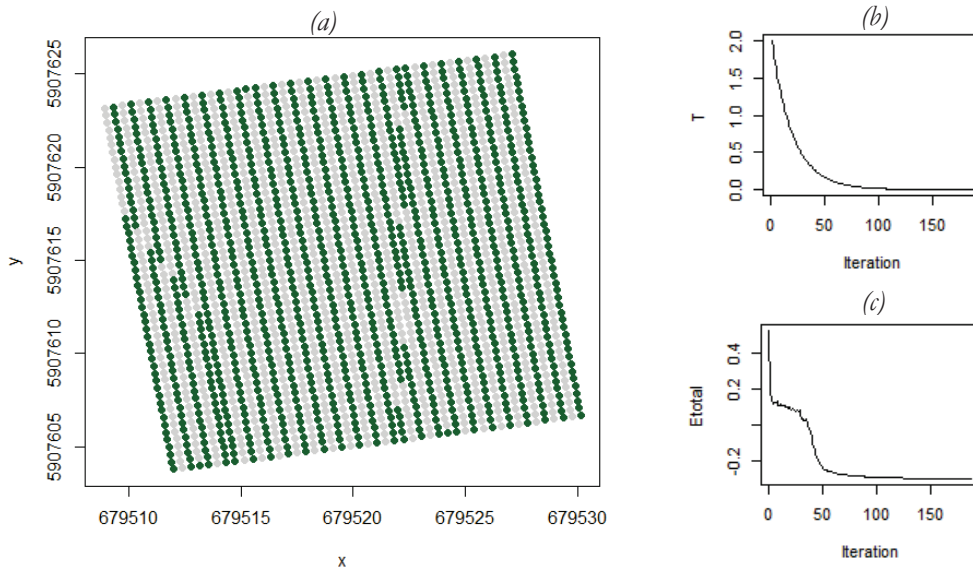


Figure 5.4: (a) Optimized SRM for window size 2 showing break lines and overlaps between consecutive rows; (b) Temperature update (c) Energy minimization curve showing local minimum values as jumps and finally converging to global minimum value below -0.2.

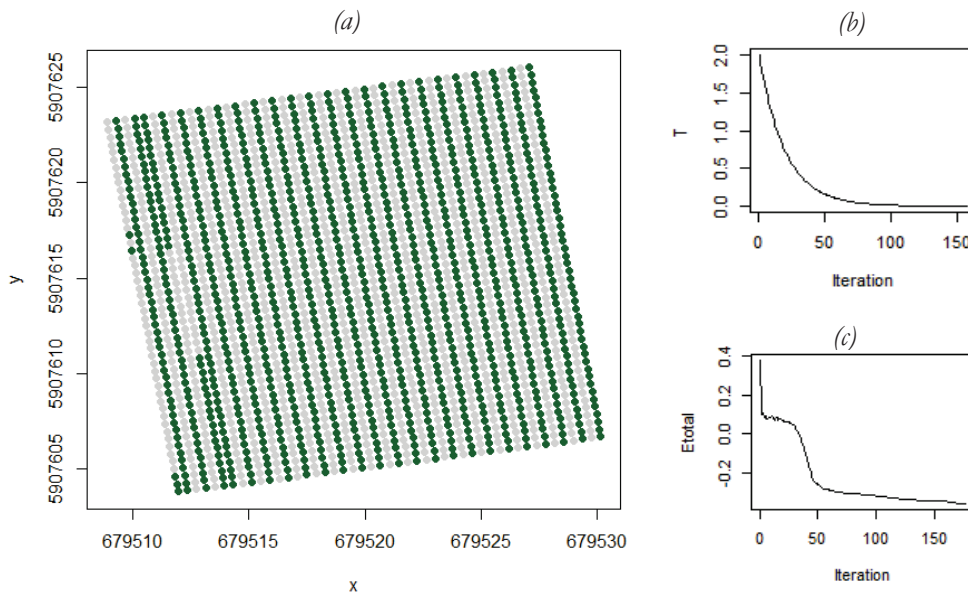


Figure 5.5: (a) Optimized SRM for window size 3 showing less break lines and overlaps between consecutive rows; (b) Temperature update (c) Energy minimization curve showing local minimum values as jumps and finally converging to global minimum value below -0.2.

Observation of above figures show that row structure are more prominent with window size 3 while more break lines occurred with window size 1 and 2. These break lines are not completely removed for window size 3 however more prominent row structure were observed. Another observation was made for the overlap of consecutive rows which is increasing in length with increase in window size. The choice of initial temperature of 2 found to be considerable, as most of the energy minimization process is occurring below temperature value of 2 with smooth cooling schedule. The occurrence of break lines and overlaps can be due to parameter settings for simulated annealing as slower annealing can lead to increased iterations and longer optimization process which can reduce the break lines and overlaps. Further experiment on simulated annealing parameters is presented in section 5.3.

Following results show the average values of 10 experiments conducted above:

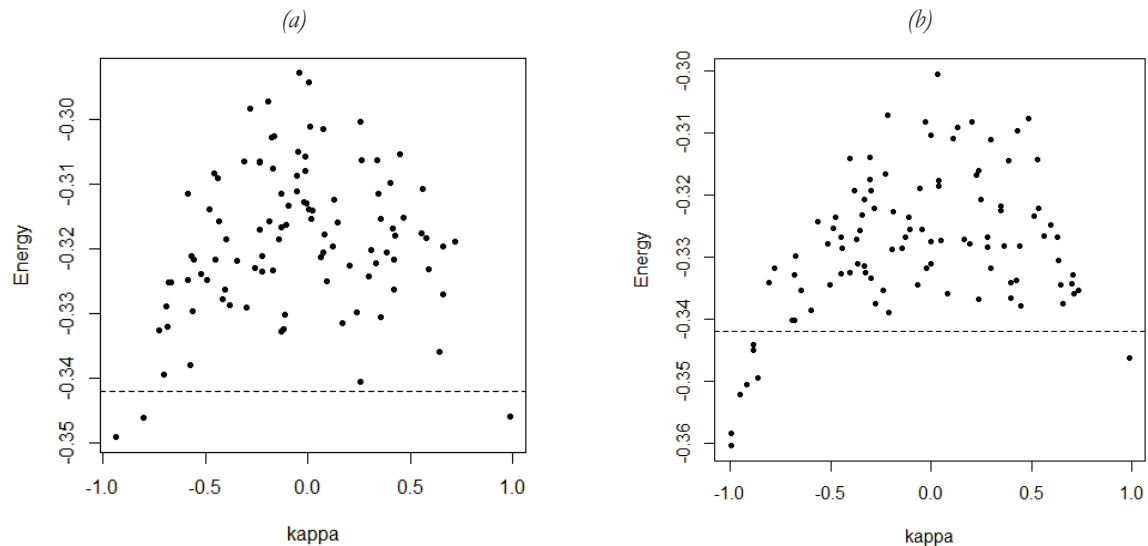
Window size	Total Energy	Prior Energy	Likelihood Energy	$k$ MLC	$k$ SRM
1	-0.291	-0.461	1.751	0.046	0.310
2	-0.334	-0.472	1.788	0.046	0.450
3	-0.354	-0.495	1.791	0.046	-0.720

Table 5.1: Average values for 10 experiments of SRM implementation for different window size

Some important observations were made from the above table. Decreasing values of average total optimized energy was found with increase in window size with lowest value at window size 3. Similar trend was observed for prior energy. However, likelihood energy showed an opposite trend with highest value at window size 3. From this experiment, window size 3 was considered to provide optimal results and used for further experiments. Most interesting observations were made on values of  $k$  as for higher window size;  $k$  value is showing strong negative results though the energy is lowest. Individual observation results of the 10 iterations showed some alarming results on accuracy of the classification as the  $k$  value was found unstable between the range of -1 and +1 for each experiment. This observation showed that though the optimized SRM is able to find the minimum energy solution with each experiment, may not be reproducible in terms of  $k$  accuracy. This issue led to further study on  $k$  statistics in relation with the minimum energy solution by increasing the number of experiments for various simulated annealing parameters.

### 5.3. Experimental results on simulated annealing parameters

Observation of  $k$  values from above experiment showed that minimum energy solution determined by the model does not necessarily correspond to higher positive  $k$  values. This issue posed a concern on the classification whether the model favours the correct solution for giving higher probability to classification with high accuracy. To address this problem, distribution of  $k$  statistics was evaluated with respect to minimum energy achieved by increasing the number of experiments for a range of simulated annealing parameters. For this experiment, same parameter settings as above were considered with  $\lambda$  0.9,  $\lambda_{pan}$  0.5,  $T_0$  2 and 100 repetitive experiments were conducted for  $T_{upd}$  values of 0.8, 0.9, 0.95, 0.99 and 0.999. Following figures show the scatterplot of minimum energy achieved for 100 iterations at different values of  $k$ .



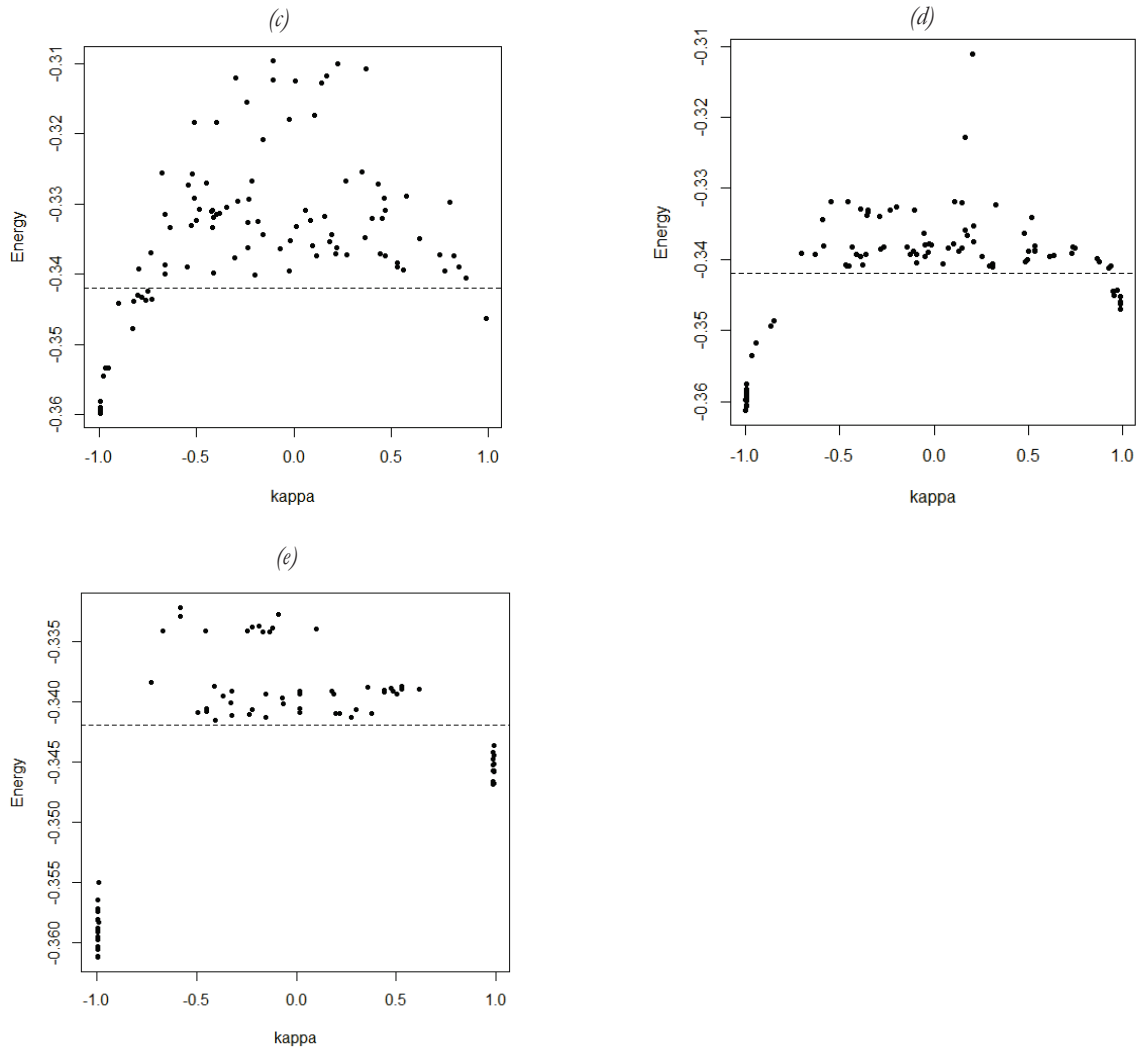


Figure 5.6: Distribution of  $k$  value at different values of  $T_{upd}$  shows high  $k$  at lowest energy values. (a)  $T_{upd}$  0.8; (b)  $T_{upd}$  0.9; (c)  $T_{upd}$  0.95; (d)  $T_{upd}$  0.99; (e)  $T_{upd}$  0.999

Observations from the above experiment show interesting findings on distribution of  $k$  values for minimum energy at different values of  $T_{upd}$ . At high values of  $T_{upd}$  0.95, 0.99 and 0.999 minimum energy is achieved with high positive and high negative  $k$  values ranging from 0.9 to 1 and -0.9 to -1.  $T_{upd}$  0.9 also show similar trend of  $k$  however the number of achievement of minimum energy corresponding to high positive or high negative  $k$  values is low. Similarly at  $T_{upd}$  0.8, few observations correspond to minimum energy solution corresponding to higher  $k$  values. At  $T_{upd}$  0.999, clear trend can be seen for distribution of  $k$  values at very high range. This proves that with very slow cooling schedule, the reproducibility of the classification is high and improved results can be achieved with high accuracy.

Another interesting observation was made on the overall range of energy in which  $k$  values are distributed. In this regard, smaller range of energy was observed for the distribution of  $k$  values for  $T_{upd}$  0.999, 0.99 and 0.95 while higher range of energy was observed for  $T_{upd}$  0.9 and 0.8. Further, for every value of  $T_{upd}$ , higher  $k$  values were observed to be distributed more towards the higher negative range than in higher positive range. This was not considered as a serious threat as the position of row classes are generated randomly by the model since no constraint has been introduced in the model for first left row being crop canopy class or soil class. This makes the model unbiased towards a particular solution.

For better evaluation of above observations, energy threshold value of  $-0.342$  was set for all values of  $T_{upd}$ . This threshold corresponds to the energy range below which higher  $k$  accuracy is observed with minimum energy and was set based on the interpretation of plots. Success rate of the classification was determined for performance evaluation of the SRM model by dividing the number of observations below threshold value by total number of observations. Following table shows the summary of above observations:

$T_{upd}$	Total energy	Observations below threshold	Iterations	Success Rate
0.999	-0.3612	52 out of 100	> 3000	0.52
0.99	-0.3612	29 out of 100	300 to 600	0.29
0.95	-0.3598	19 out of 100	150 to 300	0.19
0.9	-0.3604	8 out of 100	100 to 200	0.08
0.8	-0.3491	3 out of 100	50 to 200	0.03

Table 5.2: Summary of observations for  $k$  distribution at different values of  $T_{upd}$

Observations from the above table show that minimum energy is achieved for  $T_{upd}$  0.999 and 0.99 with highest success rate at  $T_{upd}$  0.999. Considering the slow cooling, the computation time for energy optimization at  $T_{upd}$  0.999 was found very long with number of iterations above 3000. This can be considered impractical considering the computation time. However, observations at value of  $T_{upd}$  0.999 proved that with very slow cooling, reproducibility of the results increases with highest success rate of 0.52. Comparison of minimum energy value achieved for  $T_{upd}$  0.999 and 0.99 showed that same value of minimum energy is achieved from  $T_{upd}$  0.99 with shorter computation time and with less number of iterations. Thus  $T_{upd}$  0.99 was found more practical for implementation purpose.

Based on the above table, plot for success rate of the model was generated for different  $T_{upd}$ .

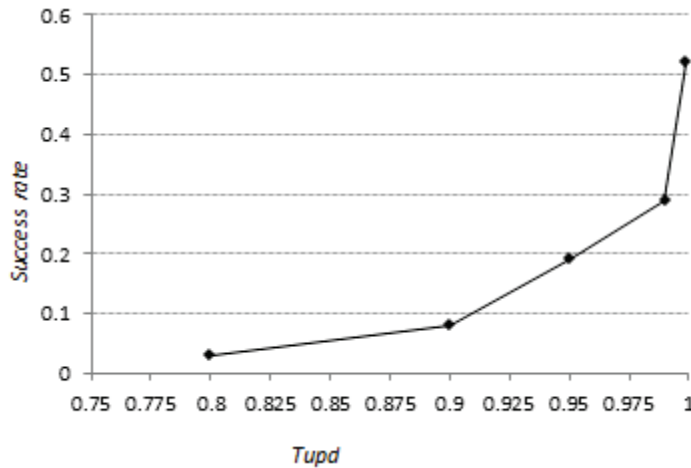


Figure 5.7: Success rate for different values of  $T_{upd}$  showing higher success rate for slower temperature updating schedule

The above experiment justifies the accuracy of SRM model in terms of its ability to produce minimum energy solution and success rate achieved for  $k$ . Distribution of high positive and high negative values of  $k$  with minimum energy for slower temperature update showed that the model favours the correct solution for giving higher probability to classification with high accuracy with slower simulated annealing. No constraint was introduced in the model for the generation of first row to a particular class. Thus, high

negative values of  $k$  indicate the generation of row classes are random as the first row can be either canopy or soil. High negative values of  $k$  also justify the reproducibility of the row structure. The rows are reproducible depending on whether the optimization process converges to a solution with first row being as canopy class or soil class.

#### 5.4. Experimental results for optimal smoothness parameter

Further experiments were conducted to determine optimal smoothness parameters for multispectral image ( $\lambda$ ) and panchromatic image ( $\lambda_{pan}$ ). Simulated annealing parameters were fixed to  $T_o$  2 and  $T_{upd}$  0.99 as justified by the above experiment. Initial experiments with  $\lambda$  value lower than  $\lambda_{pan}$  showed that energy optimization is not able to converge to a global minimum even with number of iterations more than 3000. This is mainly due to with increase in  $\lambda_{pan}$ , spectral information for panchromatic band increases. Thus high weightage on spectral information of panchromatic band alone cannot produce row structure. On the contrary, increasing the prior weight for multispectral band by increasing the value of  $\lambda$  was found to provide optimal energy solution. Considering this observation, 20 experiments were repeated for each parameter values of  $\lambda$  0.95, 0.9, 0.7, 0.5 and  $\lambda_{pan}$  0.3, 0.5. These values were set based on the accuracy of the model obtained in above experiments. Following table shows the results from the experiment:

TD	Tupd	$\lambda$	$\lambda_{pan}$	Average absolute k	Max absolute k
2	0.99	0.9	0.5	0.91	0.98
			0.3	0.79	0.95
		0.7	0.5	0.73	0.98
			0.3	0.25	0.45
		0.5	0.5	0.35	0.76
			0.3	0.42	0.65

Table 5.3: Summary of results for different smoothness parameter values

The above table shows that the average absolute value of  $k$  0.91 is highest for  $\lambda$  0.9 and  $\lambda_{pan}$  0.5 suggesting that better classification accuracy is achieved at this value. Classification accuracy starts to decrease with the decrease in  $\lambda$  which suggests that the model accuracy is more reliant on prior information from the multispectral image. The result obtained for smoothness parameter  $\lambda$  0.9 and  $\lambda_{pan}$  0.5 was also observed for row detection quality in terms of occurrence of break lines, overlap between consecutive rows and energy minimization process. Following figures show the optimized SRM for smoothness parameter values  $\lambda$  0.9 and  $\lambda_{pan}$  0.5.

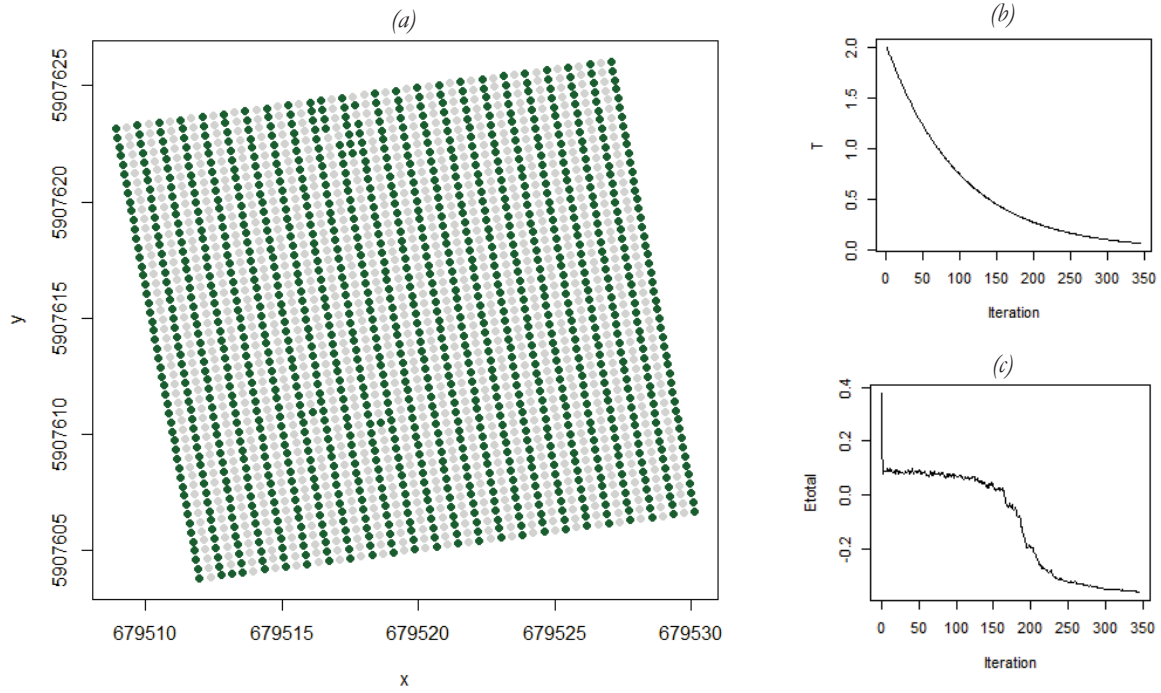


Figure 5.8: (a) Optimized SRM for  $\lambda$  0.9 and  $\lambda_{pan}$  0.5 showing best results with very few break lines and overlaps; (b) Temperature update (c) Energy minimization curve showing local minimum values as jumps and finally converging to global minimum value below -0.2.

Observation of the optimized SRM shows prominent row structure in comparison to previous experiments conducted. Very few break lines can be observed while overlaps between consecutive rows are completely removed. Energy minimization graph shows a slow decrease in energy with most of optimization occurring in the energy range between 0 and 0.2. At the starting iterations, energy decreases rapidly to range between 0.1 to 0.2 and the optimization slows down. The almost horizontal nature of graph at this range with a number of local minimum values shows the slower cooling process. Finally simulated annealing is able to find the global minimum at energy value below -0.2 at approximately 350 iterations.

From the above observations of the experimental results, this SRM model was tested for its accuracy of row detection of crop and found appropriate for even for smaller area subset of size 400 square meters. Smoothness parameters  $\lambda$  0.9 and  $\lambda_{pan}$  0.5 was found appropriate with highest  $k$  value achieved of 0.91. Simulated annealing parameters,  $T_o$  2 and  $T_{upd}$  0.99 was found appropriate. Slower cooling with longer iterations showed more accurate crop rows with less break lines and overlaps.

## 5.5. Relating SRM results with crop management

The classified row structure obtained from SRM can be a starting point for evaluation of field variations at row level. Identified rows can be combined with spectral response of vegetation through crop indicators such as NDVI or WDVI to analyse field variations. Considering the idea of using SRM results of identified rows, further exploration was done on exploiting the field variation.

Total energy of SRM corresponds to minimum energy solution to yield a maximum a posteriori (MAP) estimate. Considering the optimal smoothness parameter values, optimized posterior energy can also be related with the spectral information of image scene, as it includes likelihood energy term. Representation of this posterior energy and comparison with likelihood energy from multispectral and panchromatic bands can provide a visual perception of spectral variation that exists in field. Considering this idea, maps for total energy and likelihood energy values were created by representing the energy values with equal interval distribution with 4 category classes. Following figures show the representation map:

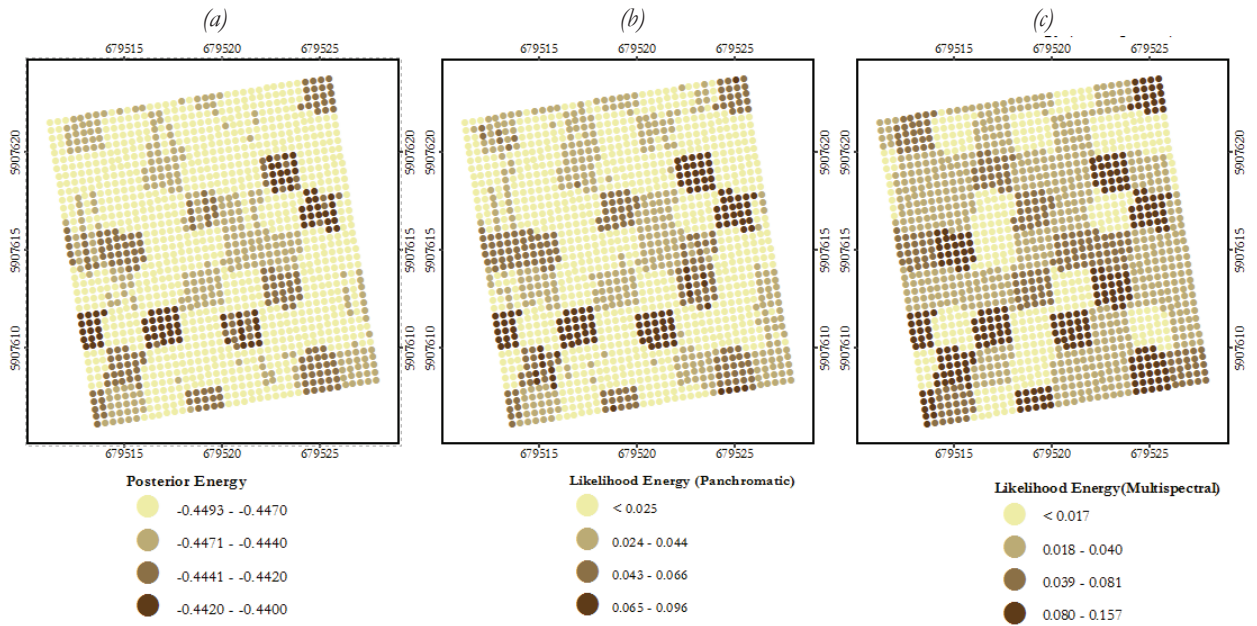


Figure 5.9: (a) Variation of SRM posterior energy within the field; (b) Variation of Likelihood energy from panchromatic band within the field; (c) Variation of Likelihood energy from multispectral band within the field

The above maps show the energy representations for SRM optimized posterior energy, likelihood energy of panchromatic band and likelihood energy of multispectral band. Classes are created based on making trials to better represent the comparison for all three energy indicators. Useful observations can be made as in most of the areas within map, energy are clustered within 5X5 pixel boxes. This is mainly due to the effect of multispectral band as the size of multispectral pixel is 5 times the resolution of SRM. Interesting observation to note is within the blocks of energy clusters variations can be seen between the energy values of pixels. This observation shows that SRM result is not biased within a pixel of multispectral image because of the varying values of energy and hence justifies the spectral variation of sub pixel fractions within one larger pixel. Posterior energy map and likelihood energy map of panchromatic band look visually similar in terms of energy distribution while likelihood energy map of multispectral band has more homogeneous pattern of clustering. This observation shows that SRM undertakes spectral information more from panchromatic image than multispectral image which also justifies the smoothness parameter settings of  $\lambda_{pan}$  0.5. Less variation and more homogeneous clustering of likelihood energy of multispectral band shows that contribution of spectral information from multispectral band is less.

To further explore the usefulness of SRM optimized energy values to observe the field variation, posterior energy map was overlaid with NDVI map created for the subset scene. This NDVI map was created

based on the band combinations of red and near infrared bands in ENVI software. Following figures show NDVI map and posterior energy overlaid over NDVI map:

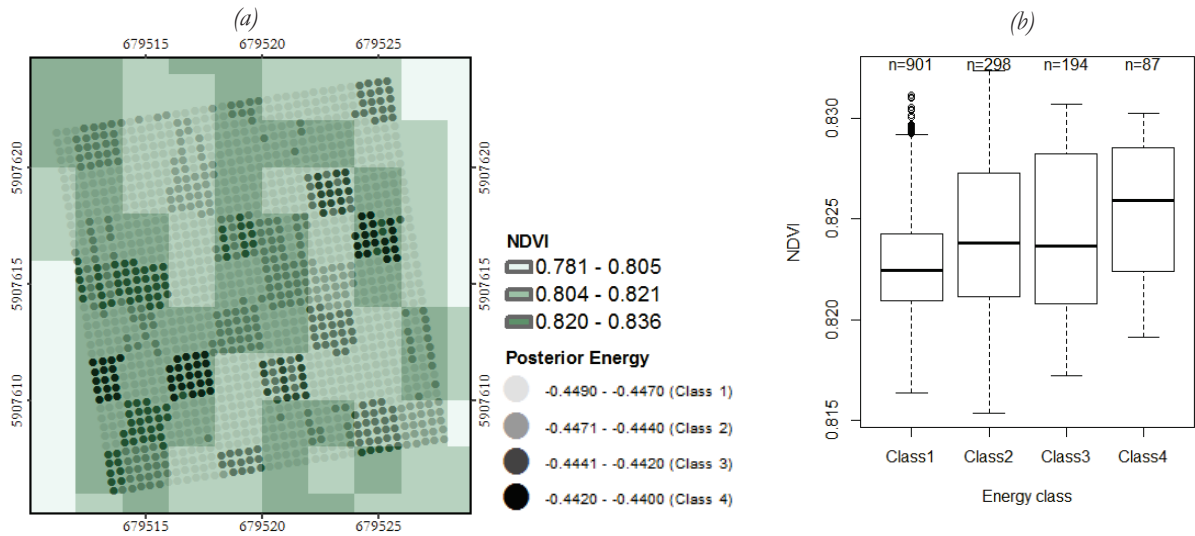


Figure 5.10: (a) NDVI map overlaid on posterior energy of SRM; (b) Box plot of showing 4 energy classes compared with NDVI values

NDVI image was classified into 3 classes based on the variation within the subset area. As can be seen from the NDVI, the subset area is mostly covered by vegetation which is shown by high NDVI values. However, the map shows some variation and as the area is small, this variation can be considerable for evaluation. Overlay map of NDVI with posterior energy grouped into 4 classes shows some useful observations. Visual inspection shows higher values of NDVI correspond to high energy as most of the dark grey pixels with higher energy lie in the region of high NDVI values while light grey pixels with lower energy values lie in the region of low NDVI values. Considering this observation, NDVI raster values were extracted to SRM posterior energy points by using ArcGIS spatial analysis extract values to point tool. To justify the above finding, box plots were created for 4 posterior energy classes against extracted NDVI. Box plots show overall increasing trend of mean values of the energy classes with increase in NDVI except for class 3 where it decreases slightly compared to class 2. However, observing the overall increasing trend of distribution of mean values with increase in NDVI, this slight decrease for class 3 was considered nominal. From this observation, it was concluded that though the range of variation of NDVI is very small with energy classes, higher posterior energy corresponds to higher NDVI values.

To further integrate the NDVI values with posterior energy for visualization purpose, ratio between posterior energy and NDVI was created. This ratio value was mapped with 3 category classes namely Zone 1, Zone 2 and Zone 3 as shown here:

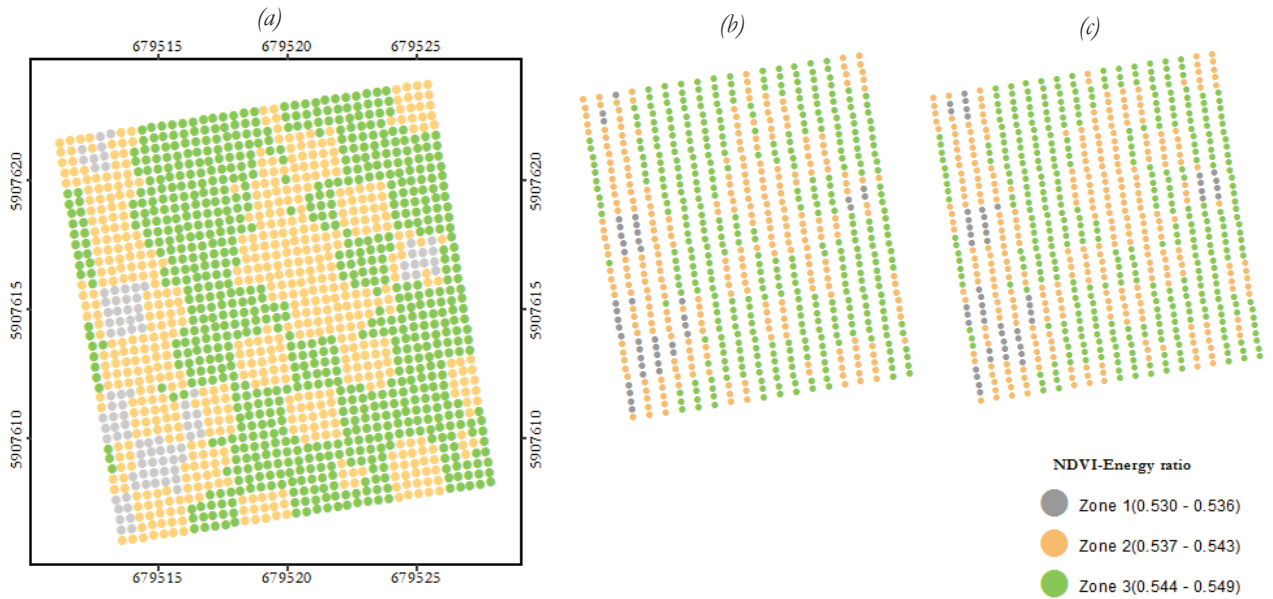


Figure 5.11: (a) Ratio map showing ratio values of NDVI with posterior energy; (b) Soil classified from SRM symbolized with NDVI-energy ratio; (c) Canopy classified from SRM symbolized with NDVI-energy ratio

The above ratio map is more informative in terms of visual evaluation of field variations as it integrates the posterior energy from SRM with NDVI values obtained from multispectral image. Visual observation shows that this map relates with the previous map of NDVI overlaid on posterior energy. From this map, it can be observed that Zone 3 with high ratio values correspond with low NDVI and low energy regions whereas Zone 1 with high ratio value range corresponds with high NDVI and high energy values. This experiment exploits the variation within field based on NDVI and energy. This NDVI-energy ratio was considered as an indicator for observing the variation within field for field areas.

Considering NDVI as major indicator for crop health, areas derived from above method can be further related to crop health and crop stress. Zone 1 with lower ratio values can be considered as healthy, Zone 2 as less healthy and zone 3 as unhealthy. However, proper field verification of this is required. Considering the time limit and scope of this work, field verification for these observations could not be conducted. Nevertheless, above findings open up possibilities for integrating SRM results with crop indicator such as NDVI. The maps show the existing field variations and can be helpful for implementation for some level of decision making. The areas such identified can also be related with management units for zone based fertilizer application, herbicide spraying and application of manure and pesticides. Further, class wise representation of the ratio values for soil and canopy row classes can be even more effective for fertilizer application for specific rows. Row maps can act as a guideline for method and amount of application of pesticides at plant level. An extended research in this direction will certainly lead to better farm management practices with the utmost use of available technology. The above findings can be considered as an initial attempt for relating SRM results with precision agriculture for better decision making.

## 6. DISCUSSION

### 6.1. Observation of the SRM results

The main objective of this study was to identify potato row crops. MRF based SRM classification with an anisotropic neighbourhood window was found to perform well. The study was challenging with respect to feature recognition, in particular considering the spatial resolution of satellite imagery, a small area for implementation with a large scale factor and in the presence of mixed pixels within the satellite image. By incorporating prior knowledge of row orientation and spacing, this study proposed SRM with an anisotropic neighbourhood window that exploits spectral and spatial information from multispectral and panchromatic imagery. This method produced an SRM based map which is independent of the initial class fraction estimation. The procedure to do so was adopted from Ardila et al. (2011) with the necessary modifications for row crop detection.

Experiments were done for implementation of neighbourhood window larger than second-order neighbourhood for a scale factor 5. Weight was assigned to the prior energy function with anisotropic expression that depends upon distance and direction of the neighbours. This property allowed detection of a significantly longer row structure with minimum number of breaks and overlaps. The lowest total energy, the highest  $k$  values and the row structure with the lowest number of break lines and overlaps for a window size of 3 justified the decision of this window size. The choice of the window size was also found justifiable in comparison to previous studies of Tolpekin et al. (2009);Kasetkasem et al. (2005). Their results indicated that for larger scale factor value such as 5, the neighbourhood order should be larger than second order as it increased the magnifying ability of the SRM.

Another exploration was done on the SRM implementation grid. As concerns the direction of rows in the subset imagery and the orientation of pixels, the SRM grid was rotated over 9 degrees to match the direction of the row structure. This allowed avoiding the rotation of the imagery subset and thus overcame the problem of pixel resampling and loss of spectral information during image rotation. Decision on target resolution of 0.4 m and representation of SRM with one pixel strip representing a single class were mainly based on prior knowledge and interpretation of pixel arrangement in image with row structure. These decisions were found justifiable from the observed optimized SRM results with inter row spacing of 0.8 m and 24 rows for a strip width of 20 m. Optimal location for row structure within rotated SRM grid was determined based on a row shift analysis. This analysis showed that for each combination of smoothness parameter values for multispectral and panchromatic band, the minimum energy is achieved at a row shift value of 0.16 m. For SRM implemented at a scale factor of 5 on small areas of 20 m  $\times$  20 m, this analysis proved to be an important achievement to decide upon the best possible location of rows within the SRM grid.

Based upon Gibbs random distribution, the minimum energy solution corresponded to an increased probability of neighbouring pixels being labelled with correct class and in this way the highest accuracy was achieved. To further evaluate this idea, the relation of minimum energy with the reproducibility of the

results from the model was evaluated by using the distribution of  $k$  accuracy. For this, a slower cooling was adopted with high values of  $T_{upd}$ . The results showed following important findings:

- Quality of detected rows increased with increasing  $T_{upd}$ . This was observed from a high  $k$  value obtained together with a relatively continuous row structure.
- The range of energy values in the distribution of the  $k$  values is small for a high  $T_{upd}$  value and vice versa.
- High  $k$  values correspond to lowest energy. Strongly negative  $k$  values show lower energy than highly positive  $k$  values.

The above findings justify the effect of slower simulated annealing on the accuracy and reproducibility of the SRM classification. With slower temperature update, the probability of pixels being labelled with the correct class increased. Therefore, SRM is able to find the minimum energy solution with a high accuracy. In this regard, a  $T_{upd}$  value equal to 0.999 showed the best results at an increased number of iterations. However, the computation time was very long, and the same value for the minimum energy was achieved with a  $T_{upd}$  value equal to 0.95. This indicates that the  $T_{upd}$  value equal to 0.999 may not be the optimal choice for practical implementation. A  $T_{upd}$  value equal to 0.99 was found appropriate as a smaller range of  $k$  values was observed, corresponding to the minimum energy, with a success rate of 0.29. This was achieved for less than 600 iterations. This is thus more practical in terms of computation time (Table 5.4). This decision was found justifiable with regard to the previous work of Ardila et al. (2011) where a  $T_{upd}$  value of 0.99 was found as an acceptable compromise between experimental accuracy obtained and computation time needed to produce SRM classification. Slower simulated annealing with  $T_{upd}$  equal to 0.99 showed a remarkable improvement in the detection quality of rows with high  $k$  values achieved at the lowest energy. A value of  $T_0$  equal to 2 was chosen based upon initial experiments and was finalized based upon the observations made on energy minimization curve where energy optimization mainly occurred below this temperature value. Lower values of  $T_0$  were not preferred as the probability of pixel update is low, thus reducing the chance of all pixels being labelled correctly. This experiment showed that with a slower temperature update, the model favours the correct solution by giving higher probability to a classification with a higher accuracy. This experiment also showed that with increased number of iterations by increasing the temperature updating schedule is a more effective way for achieving convergence with highest accuracy.

Smoothness parameter values  $\lambda = 0.9$  and  $\lambda_{pan} = 0.5$  were found appropriate in terms of the detection quality of rows and  $k$  accuracy achieved. Contribution of the panchromatic band in energy function was found significant as the results showed an improved classification accuracy for a value of  $\lambda_{pan} = 0.5$  than at lower values. Prior information is emphasized by a higher value of  $\lambda$ , whereas spectral information of imagery is incorporated from panchromatic image as  $\lambda_{pan} = 0.5$ .

## 6.2. Using the SRM results for observing field variation

Integration of the SRM results to analyse field variation within the farm is an important step forward. SRM classification results contained soil and canopy row classes with optimized energy values. These

optimized energy values included spectral information from images and were suited for a visual evaluation of field variation. Observations of the posterior energy and likelihood energy from multispectral and panchromatic bands justified this approach and showed the existence of variation in energy values within each pixel of the multispectral image. Variation of the posterior energy values corresponded more with the likelihood energy of the panchromatic image than with the multispectral image obtained from visual observation. This justified that there is a higher effect of likelihood information in the SRM classification from a panchromatic image than from a multispectral image. Variation of the posterior energy with NDVI showed an increasing trend of NDVI with increasing energy values. This finding was justified with a box plots that showed an overall increasing trend for the mean values of the energy classes with an increase in NDVI. However, this finding was made for a relatively small study area of 20m × 20m that contains small variation in NDVI values. Hence, more comprehensive research is needed for a larger area of SRM implementation containing more variation in NDVI. For visual representation, a ratio between NDVI and posterior energy was created and represented in a map with 3 classes. The map showed possibilities for representing the trend in field variation observed between NDVI and posterior energy. Higher ratio value corresponded to high energy and high NDVI and hence can be related to crop health status within the field. Field verification and further study in this direction is required.

### **6.3. Management approach for precision farming**

Farm management in precision agriculture is vital as it requires definite goals that need to be set based on farmers perception and knowledge of the farm. From farmers' perspective, these goals mainly include profitability, product quality, risk reduction and environmental protection (Lake et al., 1997). A new generation of farmers should be promoted based on their capability for decision making on how they prefer to handle their farm based on their own knowledge. As a scientist, the challenge is to properly adopt the idea of 'performance evaluation' than 'design evaluation' and develop a management system that incorporates environmental threshold values for performance evaluation in a variable medium of time and space. The overall idea is to place farmers in the first place for decision making by allowing them to take decisions based on 'what' they want to do 'when' and 'where'. This concept was found more relevant for current agricultural practices and is presented by Johan Bouma in his general reflections over a discussion of precision agriculture symposium (Lake et al., 1997). He presented a 'management toolkit' for the farmers that shows two major tracks namely: a forward looking approach and a backward looking approach with different elements within the toolkit that can be applied at different time and location during the cropcycle.

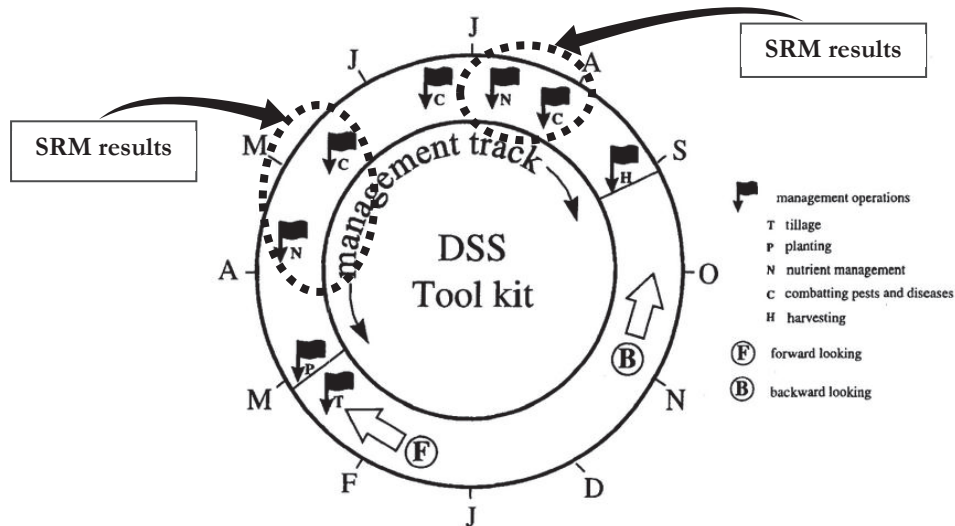


Figure 6.1: Management toolkit for the management track of potatoes showing possible integration of SRM results for management operations. Source: (Lake et al., 1997)

Considering the traditional approaches for crop management that incorporates management in time such as in application of fertilizer at different period of crop growth, this toolkit integrates the concept of management in space and time such as in observing the within farm variation to applications of specific measures at particular farm locations. He suggested that both forward and backward looking approaches should be adopted and that the elements of the toolkit can be applied at different times and spaces for better (i.e. higher and/or environmentally friendly) productivity. This decision can be made by farmers based on the knowledge of their own field and existing management practice. The above figure shows possible integration areas of SRM results within the particular management operations of the toolkit.

The management toolkit explores the possibilities of the use of remote sensing data for decision support. The results obtained from analysis of the field variation can be supportive and hence can be integrated into the management operations. More specifically, our SRM output can be included into management operations such as in nutrient management. Nutrient management is the system for managing the optimal amount of nutrients to plants at the right location and the right time. It helps to prevent runoff of pollutants to surface water thus maintaining the quality of soil. Integrating knowledge of variation of crop obtained from combining SRM results and NDVI can support in decision making on the amount and location of nutrient required at row level. Farmers will be able to take decisions on varying nutrient application and can be able to answer questions such as at which particular row location nutrient should be applied to what amount. In this way integration of SRM results into nutrient management can help for better management of crops. Further, SRM results of field variation can be an indicator of crop stress and can be supportive in making decisions for nutrient application based on variation of water content availability of the farm field. For making decisions on combating pests and diseases, SRM results combined with NDVI can be related with the crop health status. By evaluating the variation of crop health status at each particular row location, decisions can be made on amount and location of spraying the right amounts of herbicides and pesticides.

Remote sensing has relatively long history in precision farming. Observation of spatial variations in field using crop indicators such as NDVI, WDVI has been done in past and are still under research. One of the recent concerns in precision agriculture is the level of detail in which we can exploit a particular field for

variation using the remote sensing technologies. In this regard, this study has opened up possibilities for looking inside the field particularly at row level for plant monitoring and management. Further extension to this can be the identification of individual plants and monitoring the variation at individual plant level within a field. This however, requires images with higher spectral quality with better spatial resolution in high temporal resolution. High spatial resolution time series images can provide continuous monitoring of the same area at different time with higher accuracy. In the meantime, the approach should be the use of latest and cost effective available technology. High resolution aerial sensors such as UAV (Unmanned aerial vehicle) can provide appropriate solutions for acquiring images at better spatial and temporal resolution at lower cost. With greater temporal accuracy images, decisions can be made at different time of the crop growing season at plant level. This approach can certainly lead to efficient monitoring of farm field at individual plant level thus strengthening the existing crop management practices.

#### 6.4. Answers to the research questions

- What are the basic criteria for site selection and identifying specific potato farms in the proposed site from satellite imagery?

With review of available sensors, imagery selection was done mainly considering the capture date, available bands, coverage of study area and other important image attributes. Selection of site within image was done based on field verification of sites that were initially identified on desk study. Details are presented in section 4.1.2 and 4.1.3.

- How to utilize prior knowledge of periodic spatial structure in SRM?

Prior knowledge of field was incorporated in SRM model as inter row spacing, alignment of rows and location of boundaries.

- What spectral classes should be defined before implementation of SRM?

Crop canopy and soil classes were defined based on the field verification

- What are the optimal parameter settings to obtain the best SRM result?

As observed from results,  $\lambda$  0.9,  $\lambda_{pan}$  0.5,  $T_0$  2 and  $T_{upd}$  0.99 were found the optimal parameter settings.

- Is it possible to identify individual rows of potatoes at field level using MRF based SRM?

It was found that even for complex scenes with high mixed pixels, SRM implemented with anisotropic prior model with larger window size is able to identify plant rows with prior information from field and spectral information from image data.

- How to validate the classification output?

Validation of classification output was done with  $k$  accuracy and success rate of the model to reproduce the same result.

- What management recommendations can be identified for site specific management for better application of manure and pesticides?

This study being limited in terms of time and resources, is not able to recommend quantitative indicators for better management of farm. However, recommendations have been derived based on SRM results and literature review. Major aspect for management that should be preferred is to place farmer in first position for decision making. Details are provided in section 7.2

- Does SRM provide more information on spectral variation of field than crop indicators such as NDVI?

Map of the SRM energy values showed that variation can be observed at finer level than the existing multispectral image as it was observed that within each pixel of multispectral image, variation in energy exists. Further, relating energy values with NDVI justified that SRM can provide more information on spectral variation than crop indicators such as NDVI.

## 7. CONCLUSION AND RECOMMENDATIONS

### 7.1. Conclusion

In this research, MRF based SRM with anisotropic prior was implemented for a potato farm field of area 20m X 20m. Class statistics were mainly derived from the imagery pixels with updates using linear mixture model from class area proportion assumptions made based on the field knowledge and measurement. SRM implemented in this research differ in following areas with the previous similar works:

- The coordinate grid of SRM was rotated with respect to the image subset grid.
- The link between pixels of rotated SRM grid and non-rotated pixels of image were established through geographic coordinates.
- SRM was implemented with anisotropic prior for a non-integer scale factor value.

Neighbourhood window size of 3 with appropriate parameter settings is able to identify potato crop rows with less break lines and overlaps. From the observation of results, smoothness parameter values  $\lambda$  0.9 and  $\lambda_{pan}$  0.5 were found to provide optimal solutions while slower simulated annealing with  $T_o$  2 and  $T_{upd}$  0.99 produced continuous row structure. Following major conclusions were derived from the observation of results:

- SRM grid with row shift of 0.16m corresponds to minimum energy solution for this implementation. This analysis should be done beforehand for implementation in other areas of the field as the energy values differ with the location of study area.
- Slower simulated annealing increases probability of pixels being labelled with correct class. Higher accuracy can be achieved with slower temperature update.
- Reproducibility of row classes depends on the ability of an optimization process to converge towards a solution with first row being as canopy class or soil class.

Posterior energy compared with NDVI obtained from multispectral image showed possibilities for integrating the SRM results for precision crop management. Field level variation can be observed by combining the SRM posterior energy with NDVI. This variation can be supportive in better decision making in terms of pest application and herbicide spraying at row level. To fulfil the management goals, farmers' perspective towards the management should be made first priority.

### 7.2. Recommendations

Major challenge faced during this research was in proper addressing of the mixed pixels effect in the imagery. Considering the spatial resolution of the panchromatic image of 0.5m, and the approximate crop canopy diameter of 0.4m, overlap between the plant canopy crowns and interlocking between rows created large amount of mixed pixels. This was observed during determination of class statistics for soil and canopy as pure pixels for both classes could not be determined in image. To tackle this problem, class statistics obtained from mixed pixel training classes were refined with linear unmixing model. Assumption was made on the class area proportion for soil and canopy based on field knowledge. This method is also

recommended by (Tolpekin et al., 2009) for refining training set including mixed pixels with known class area proportions. In implementation, the SRM grid was rotated to avoid the loss of spectral information that can occur due to resampling of image pixels during rotation. In this context, this study also exploits possibility for handling large mixed pixel effect in potato farm field.

For the area containing pure pixels of soil and canopy, a slightly different approach should be adopted. Considering the high importance of soil reflectance for precision agriculture, soil correction should be made for pure training pixels of collected soil. Estimation of soil line from pure pixels of red and NIR bands on image provides exact determination of soil location within the scatterplot. This scatterplot should be used for finalization of class statistics based on the spectral separability of classes. Further, estimation of soil line slope also helps in determining the soil corrected vegetation indices such as WDVI. From literature, it was found that WDVI can be better vegetation index for crops such as potato as it incorporates soil correction. This approach is further recommended for the implementation area containing pure pixels of soil and canopy.

Due to the scope of work and limited time frame, field verification could not be conducted for the observations made from integrating SRM energy for exploiting field variation. Further detailed analysis with proper field verification is recommended in this direction.

Crop growth model provides a comprehensive framework for efficient management of farm and hence detail study is recommended. The results obtained from this study can be integrated to a crop growth model for better estimation of number of crop canopy variables such as fraction of absorbed photosynthetic stress (fAPAR), Leaf area index (LAI) etc. Estimation of crop biomass, crop stress and health status can be systematically modelled with crop growth model.

Detail study of crop management in precision agriculture with the management toolkit is further recommended. In this research only a limited review of management toolkit for the farmers was done and based on this, following recommendations can be made for the farmers to achieve their specific goals:

- Both forward looking and backward looking approach should be adopted based on the time of crop growing season.
- Manipulation in nutrient management (N, K, P) by using manure and fertilizer should be done considering the spatial variation within farm.
- Row level variation maps should be used for better management decisions on nutrient management and combating pests and diseases.

## LIST OF REFERENCES

- Ardila, J. P., Tolpekin, V. A., Bijker, W., & Stein, A. (2011). Markov-random-field-based super-resolution mapping for identification of urban trees in VHR images. [Article]. *Isprs Journal of Photogrammetry and Remote Sensing*, 66(6), 762-775.
- Atkinson, P. M. (2004). *Super-resolution land cover classification using the two-point histogram* (Vol. 13). Dordrecht: Springer.
- Atkinson, P. M. (2005). Sub-pixel target mapping from soft-classified, remotely sensed imagery. [Article]. *Photogrammetric Engineering and Remote Sensing*, 71(7), 839-846.
- Atkinson, P. M. (2009). Issues of uncertainty in super-resolution mapping and their implications for the design of an inter-comparison study. *International Journal of Remote Sensing*, 30(20), 5293-5308.
- Atkinson, P. M., Cutler, M. E. J., & Lewis, H. (1997). Mapping sub-pixel proportional land cover with AVHRR imagery. [Article; Proceedings Paper]. *International Journal of Remote Sensing*, 18(4), 917-935.
- Bauer, M. E. (1985). Spectral inputs to crop identification and condition assessment. [Article]. *Proceedings of the Ieee*, 73(6), 1071-1085.
- Boucher, A., Kyriakidis, P. C., & Cronkite-Ratcliff, C. (2008). Geostatistical solutions for super-resolution land cover mapping. [Article]. *Ieee Transactions on Geoscience and Remote Sensing*, 46(1), 272-283.
- Bouman, B. A. M. (1995). Crop modeling and remote-sensing for yield prediction. [Article]. *Netherlands Journal of Agricultural Science*, 43(2), 143-161.
- Brown, M., Gunn, S. R., & Lewis, H. G. (1999). Support vector machines for optimal classification and spectral unmixing. [Article]. *Ecological Modelling*, 120(2-3), 167-179.
- Campbell, J. B. (2002). *Introduction to Remote Sensing, 3rd Edition*: Taylor & Francis Group.
- Clevers, J. G. P. W. (1988). The derivation of a simplified reflectance model for the estimation of Leaf-Area Index. [Article]. *Remote Sensing of Environment*, 25(1), 53-69.
- Clevers, J. G. P. W. (1997). A simplified approach for yield prediction of sugar beet based on optical remote sensing data. *Remote Sensing of Environment*, 61(2), 221-228.
- De Jong, S. M. d., & Meer, F. v. d. (Eds.). (2006). *Remote sensing image analysis: including the spatial domain Remote sensing and digital image processing v. 5*. DE: Springer Verlag.
- Foody, G. M. (2002). Status of land cover classification accuracy assessment. [Review]. *Remote Sensing of Environment*, 80(1), 185-201.
- Foody, G. M., & Cox, D. P. (1994). Sub-pixel land-cover composition estimation using a linear mixture model and fuzzy membership functions. [Article]. *International Journal of Remote Sensing*, 15(3), 619-631.
- Haboudane, D., Miller, J. R., Tremblay, N., Zarco-Tejada, P. J., & Dextraze, L. (2002). Integrated narrow-band vegetation indices for prediction of crop chlorophyll content for application to precision agriculture. [Article]. *Remote Sensing of Environment*, 81(2-3), 416-426.
- Hatfield, J. L., & Pinter, P. J. (1993). Remote-sensing for crop protection. [Review]. *Crop Protection*, 12(6), 403-413.
- Hong, N., White, J. G., Weisz, R., Crozier, C. R., Gumpertz, M. L., & Cassel, D. K. (2006). Remote Sensing-informed Variable-rate Nitrogen Management Of Wheat And Corn. *Agron. J.*, 98(2), 327-338.
- Kasetkasem, T., Arora, M. K., & Varshney, P. K. (2005). Super-resolution land cover mapping using a Markov random field based approach. [Article]. *Remote Sensing of Environment*, 96(3-4), 302-314.
- Kassaye, H. R. (2006). *Suitability of Markov random field based method for super resolution land cover mapping*. ITC, Enschede. Retrieved from [http://www.itc.nl/library/papers\\_2006/msc/gfm/hailu.pdf](http://www.itc.nl/library/papers_2006/msc/gfm/hailu.pdf)
- Lake, J. V., Bock, G., Goode, J., Organisation, E. E. R., & Foundation, C. (1997). *Precision agriculture: spatial and temporal variability of environmental quality*. Wiley.
- Mertens, K. C., Verbeke, L. P. C., Westra, T., & De Wulf, R. R. (2004). Sub-pixel mapping and sub-pixel sharpening using neural network predicted wavelet coefficients. [Article]. *Remote Sensing of Environment*, 91(2), 225-236.
- Moran, M. S., Inoue, Y., & Barnes, E. M. (1997). Opportunities and limitations for image-based remote sensing in precision crop management. *Remote Sensing of Environment*, 61(3), 319-346.
- Richards, J. A., & Jia, X. (2005). *Remote Sensing Digital Image Analysis: An Introduction*: Springer.

- Tatem, A. J., Lewis, H. G., Atkinson, P. M., & Nixon, M. S. (2003). Increasing the spatial resolution of agricultural land cover maps using a Hopfield neural network. [Article]. *International Journal of Geographical Information Science*, 17(7), 647-672.
- Tatem, A. J., Lewis, H. G., Atkinson, P. M., Nixon, M. S., & Ieee. (2001). *Super-resolution mapping of urban scenes from IKONOS imagery using a Hopfield neural network*. New York: Ieee.
- Tolpekin, V. A., & Stein, A. (2009). Quantification of the effects of land - cover - class spectral separability on the accuracy of Markov - random - field - based superresolution mapping. *JournalIEEE Transactions on geoscience and remote sensing*, 47(9), 3283-3297.
- Tso, B., & Olsen, R. C. (2005). A contextual classification scheme based on MRF model with improved parameter estimation and multiscale fuzzy line process. *Remote Sensing of Environment*, 97(1), 127-136.
- van Evert, F. K., van der Voet, P., van Valkengoed, E., Kooistra, L., & Kempenaar, C. (2012). Satellite-based herbicide rate recommendation for potato haulm killing. [Article]. *European Journal of Agronomy*, 43, 49-57.
- Verhoeve, J., & De Wulf, R. (2002). Land cover mapping at sub-pixel scales using linear optimization techniques. [Article]. *Remote Sensing of Environment*, 79(1), 96-104.
- Wu, B. F., Meng, J. H., Li, J. Z., Zhang, F. F., Du, X., Niu, L. M., & Zhang, M. A. (2010). A pilot study for the application of remote sensing in precision farming. In H. Guo & C. Wang (Eds.), *Sixth International Symposium on Digital Earth: Data Processing and Applications* (Vol. 7841). Bellingham: Spie-Int Soc Optical Engineering.